Cell Plasticity in a Mouse Model of Benign Prostate Hyperplasia Drives Amplification of Androgen-Independent Epithelial Cell Populations Sensitive to Antioxidant Therapy

Leïla dos Santos, Francesco Carbone, Emeline Pacreau, Sekou Diarra, Marine Luka, Natascha Pigat, Manon Baures, Emilie Navarro, Julien Anract, Nicolas Barry Delongchamps, et al.

The American Journal of Pathology, Vol. ■, No. ■, ■ 2023

The American Journal of PATHOLOGY
ajp.amjpathol.org

Cell Plasticity in a Mouse Model of Benign Prostate Hyperplasia Drives Amplification of Androgen-Independent Epithelial Cell Populations Sensitive to Antioxidant Therapy

Leïla Dos Santos,* Francesco Carbone,[†‡] Emeline Pacreau,* Sekou Diarra,[§] Marine Luka,*[†] Natascha Pigat,* Manon Baures,* Emilie Navarro,* Julien Anract,*[¶] Nicolas Barry Delongchamps,*[¶] Nicolas Cagnard,[‖] Frédéric Bost,[**] Ivan Nemazanyy,[††] Olivier Petitjean,[‡‡] Ahmed Hamaï,* Mickaël Menager,[††] Stefano Palea,[§] Jacques-Emmanuel Guidotti,* and Vincent Goffin*

From the Institut Necker Enfants Malades, Université Paris Cité, INSERM UMR-S1151, CNRS UMR-S8253, Paris; Laboratory of Inflammatory Responses and Transcriptomic Networks in Diseases,[†] Imagine Institute, Université Paris Cité, Atip-Avenir Team, INSERM UMR 1163, Paris; Labtech Single-Cell@Imagine,[‡] Imagine Institute, INSERM UMR 1163, Paris; Humana Biosciences SAS,[§] Prologue Biotech, Labège; Urology Department,[¶] Hôpital Cochin, Assistance Publique Hôpitaux de Paris, Paris; Bioinformatics Core Platform,[‖] Université Paris Cité, INSERM UMR1163 and Structure Fédérative de Recherche Necker, INSERM US24/CNRS UAR3633, Paris; C3M,** INSERM U1065, Université Côte d'Azur, Equipe Labélisée Ligue Nationale contre le Cancer, Nice; Metabolomics Core Facility,[††] Université de Paris - Structure Fédérative de Recherche Necker, INSERM US24/CNRS UAR3633, Paris; and Zion Pharma,[‡‡] Marseille, France

Accepted for publication September 12, 2023.

Address correspondence to Vincent Goffin, INEM Team 5, Faculté de Médecine Necker, 160, rue de Vaugirard, Paris, France.
E-mail: vincent.goffin@inserm.fr.

Benign prostate hyperplasia (BPH) is caused by the nonmalignant enlargement of the transition zone of the prostate gland, leading to lower urinary tract symptoms. Although current medical treatments are unsatisfactory in many patients, the limited understanding of the mechanisms driving disease progression prevents the development of alternative therapeutic strategies. The probasin-prolactin (Pb-PRL) transgenic mouse recapitulates many histopathological features of human BPH. The authors show these alterations parallel urodynamic disturbance reminiscent of lower urinary tract symptoms. Single-cell RNA-sequencing analysis of Pb-PRL mouse prostates revealed that their epithelium mainly includes low-androgen signaling cell populations analogous to Club/Hillock cells enriched in the aged human prostate. These intermediate cells are predicted to result from the reprogramming of androgen-dependent luminal cells. Pb-PRL mouse prostates exhibit increased vulnerability to oxidative stress due to reduction of antioxidant enzyme expression. One-month treatment of Pb-PRL mice with anethole trithione (ATT), a specific inhibitor of mitochondrial ROS production, reduced prostate weight and voiding frequency. In human BPH-1 epithelial cells, ATT decreased mitochondrial metabolism, cell proliferation and stemness features. ATT prevented the growth of organoids generated by sorted Pb-PRL basal and LSC^{med} cells, the two major BPH-associated, androgen-independent epithelial cell compartments. Taken together, these results support cell plasticity as a driver of BPH progression and therapeutic resistance to androgen signaling inhibition, and identify antioxidant therapy as a promising treatment of BPH. *(Am J Pathol 2023, ■: 1–22; https://doi.org/10.1016/j.ajpath.2023.09.010)*

Benign prostatic hyperplasia (BPH) is a common disease characterized by the nonmalignant hyperproliferation of the stromal and/or glandular cell compartments in the transition zone of the prostate, leading to bladder outlet obstruction and lower urinary tract symptoms (LUTS).[1,2] LUTS are particularly prevalent in the aging population and markedly

Partly funded by Inserm (V.G.), University Paris Cité (V.G.), CNRS (V.G.), and the Agence National de la Recherche grant ANR-22-CE14-0059-01 (V.G.). L.D.S. was supported by a CIFRE PhD fellowship (Zion Pharma and Association Nationale Recherche Technologie (ANRT), contract n°191037A10) and Association Endocrinologie Clinique et Recherche (ECLER). M.B. was supported by a Ph.D. fellowship from the Ministry of Research.

https://doi.org/10.1016/j.ajpath.2023.09.010

affect the quality of life of patients.[2,3] The only etiologic treatment of LUTS involves 5α-reductase inhibitors (5-ARIs) that block intraprostatic conversion of testosterone into its active metabolite dihydrotestosterone, leading to apoptosis of androgen-dependent cells of the glandular epithelium.[4] Although up to 25% prostate size reduction can be observed after 1-year treatment,[2,4] approximately half of the patients are unsatisfactorily treated due to incomplete clinical response or resurgence of BPH progression within 4 years.[5,6] Moreover, 5-ARIs induce a range of side effects (decreased libido, erectile dysfunctions, and gynecomastia), strongly reducing patient compliance in the long term.[7]

Oxidative stress is commonly associated with age-related diseases,[8] including BPH.[9,10] Hallmarks of oxidative stress (eg, malondialdehyde, peroxidized lipids, carbonylated proteins) are elevated in serum[11,12] and/or in the prostatic epithelium of BPH patients.[10,13,14] These features parallel prostate weight and are inversely correlated to the activity of antioxidant enzymes such as catalase and glutathione peroxidases in the prostatic tissue.[10,13,14] The actual role of oxidative stress in BPH pathogenesis is poorly understood, and the potential benefit of antioxidant therapy in preclinical models of BPH is unexplored.

The probasin-prolactin (Pb-PRL) transgenic mouse[15] recapitulates the autocrine/paracrine prolactin (PRL) signaling loop shown to promote epithelial cell growth and survival in the human prostate.[16,17] Pb-PRL mice exhibit several features of human BPH including progressive development of tissue hypertrophy with increased stromal cellularity, immune cell infiltration, epithelial cell hyperplasia, and intraepithelial neoplasia.[15,17–22] The hypertrophied Pb-PRL mouse prostate is enriched in a peculiar cell population called LSC^{med}.[23,24] LSC^{med} defines nonsecretory luminal cells[25] that exhibit a specific transcriptomic profile enriched in stemness markers (*Psca*, *Tacstd2*, *Cd44*, *Sox2*, *Sca-1*),[23] and are able to generate organoids *in vitro* and glandular epithelium *in vivo*.[24,26,27] Importantly, LSC^{med} cells are tolerant to androgen deprivation.[23,26,28] LSC^{med} cells show molecular similarity with Club cells of the human prostate.[27,28] Club cells have been proposed to be urethral cells that extend into the proximal ducts of the prostate transition zone, where BPH develops.[29] They are enriched in BPH compared with healthy prostate,[30,31] and this phenotype is aggravated by 5-ARI treatment, which was proposed to result from luminal cell reprogramming into Club-like cells.[32] Together, these observations suggest that cells exhibiting LSC^{med}/Club-like features may contribute to BPH development and therapeutic resistance.

Based on its human BPH-related hallmarks, the Pb-PRL mouse is emerging as one of the most relevant preclinical BPH models.[28,33,34] As such, it has been used to challenge new therapeutic options for BPH.[34,35] In keeping with this, the first aim of this study was to use single-cell RNA sequencing (scRNAseq) to elucidate the complex cell composition of hypertrophied Pb-PRL prostates and progress in our understanding of BPH pathobiology. This analysis revealed the emergence of various low-androgen signaling cell states intermediate between basal and luminal lineages, suggesting epithelial cell plasticity reminiscent of what has been hypothesized in the human disease. The second aim was to explore the therapeutic benefit of antioxidant therapy for the treatment of BPH.

Materials and Methods

Mice

The Pb-PRL mouse carries the rat prolactin transgene driven by the prostate-specific short probasin promoter.[15,19,23] Colonies established on *C57BL/6J* background were housed on a 12:12 hour light/dark cycle with normal chow diet. Information on experimental animals (*Pb-Prl*$^{+/-}$) used in this study (number, age, housing) is reported in Table 1. All experiments were [T1] approved by local ethical committees for animal experimentations (APAFIS#18297-2018032710526065 v2 and APAFIS#12547-2017112008275221 v7).

Antioxidant Treatment

Anethol trithione (ATT) was supplied by Zion Pharma (Marseille, France) as an orange/brown powder (raw material for SULFARLEM, purity 98.7% produced by M2I SALIN, Salin de Giraud, France, lot GIG203503).

For animal studies, ATT was resuspended extemporaneously in pure coconut oil (C1758-500G; Sigma-Aldrich, Saint-Quentin-Fallavier, France) at a concentration of 15 mg/mL. The effects of antioxidant therapy on urodynamic and cellular/molecular parameters of Pb-PRL mice were determined after 30 days of daily oral treatment with ATT (60 mg/kg/day) versus vehicle (coconut oil). This dosing allows a T_{12h} plasma concentration (approximately 150 ng/mL, as determined by mass spectrometry) similar to what is observed in humans after 75 mg oral dosing.[36] For cell studies, ATT was dissolved in pure dimethyl sulfoxide (DMSO) at a concentration of 10 mmol/L, aliquoted, and then stored at −20°C. As needed, it was diluted in culture medium and applied onto cell cultures at a final concentration of 10 μmol/L versus similarly diluted DMSO (vehicle). Higher concentrations of ATT (20 μmol/L and above) were found to precipitate in culture medium (formation of crystals).

Urodynamic Parameters

Urodynamic parameters were determined at Humana Biosciences (CREFRE, Toulouse, France) using specialized metabolic cages (Shinfactory, Fukuoka, Japan)[37] installed in a separate quiet room of the animal facility. The floor of each cage consists of a patented mesh that allows urine to pass through but traps feces. A square-shaped water-repellent funnel positioned below the mesh directed voided urine that passed through it into a container located on a precise

FLA 5.6.0 DTD ■ AJPA3976_proof ■ 22 October 2023 ■ 9:32 am ■ EO: AJPA-D-23-

Table 1 *In Vivo* Experimentation

Experiment	Mice	Housing
Urodynamic tests		
Pb-PRL phenotype	17 Pb-PRL versus 15 WT (4—7-month—old, ie, established BPH)	CREFRE (Toulouse), SOPF health status
ATT treatment	11 ATT-treated Pb-PRL versus 12 vehicle-treated Pb-PRL (12—14-month—old, ie, advanced BPH)	
scRNAseq	2 vehicle-treated Pb-PRL (#504, #756) versus 2 ATT-treated Pb-PRL (#506, #748) (6—8-month—old, ie, established BPH)	LEAT (Broussais site), conventional health status
Affymetrix of sorted epithelial cells	3 Pb-PRL mice (6—8-month—old, ie, established BPH)	
Other studies (organoids, RT-qPCR, immunoblots, immunohistochemistry, cell sorting)	Pb-PRL and WT mice (6—8—month-old, ie, established BPH)	LEAT (Broussais and Necker sites), conventional health status

balance meter (GX-1003A; A&D Company Ltd., Tokyo, Japan). Quantities of water and food sufficient to last for a few days were prepared for administration through the supply line and feeder box, respectively. Food and water were *ad libitum*.

Basal urodynamic parameters were determined by putting mice in these metabolic cages for 48 hours. The first 24 hours allowed animal acclimatization to their new environment. After the acclimation period, data on voided urine (weight and timing) and water consumption (volume and timing) were continuously collected for each mouse over a further 24 hours using a Micro1401 data acquisition system (Cambridge Electronic Design, Milton, Cambridge, UK). Data were converted by a digitizer to digital signals and entered into a computer for analysis by Spike II software (Cambridge Electronic Design). Data include food intake (g/day), water intake (mL/day), urine output volume (mL/day), voiding frequency (times/dark period and/light period), urine volume per voiding (μL), voiding duration (seconds), and mean uroflow rate (μL/second) calculated as the urine volume per voiding (μL)/voiding duration (seconds).

Before starting the chronic treatment of Pb-PRL mice with ATT, the basal urodynamic parameters were determined as described above for each Pb-PRL mouse. Following this step, daily treatment by oral route with ATT or vehicle was started. ATT (15 mg/mL) was administered at 10 mL/kg by oral gavage (60 mg/kg/day) once a day between 9 and 11 AM, for 30 consecutive days. Due to the lack of administration of the drug on Sunday, a double dose of ATT (120 mg/kg) was administered on Saturday mornings (the half-life of ATT following oral administration in mice is around 30 minutes). On the 29th day, mice were again transferred into metabolic cages for acclimatization and stabilization of urodynamic parameters (24 hours) before measurements of urodynamic parameters for each mouse (next 24 hours). ATT was administered during the first and second days of permanence in the metabolic cages. At the end of urodynamic recordings, mice were euthanized by cervical dislocation, and exsanguination was performed by sectioning of the abdominal aorta. Urogenital tissues (urinary bladder, urethra, anterior prostates, and whole prostate) were gently blotted on a filter paper and weighted using an electronic microbalance. Organ weights are expressed as a function of each mouse body weight. Results are presented as means ± SD using statistical tests as indicated in the figure captions. All differences were considered statistically significant when the null hypothesis can be rejected at a risk α of <0.05.

Single-Cell RNA-Sequencing

Prostates of four Pb-PRL mice treated for 30 days with vehicle ($n = 2$) or ATT ($n = 2$) (Table 1) were harvested, carefully excluding the urethra. Prostate tissue was dissected and digested as described,[38] then dead cells (SYTOX Blue-positive) and Ter119-positive cells (erythrocytes) were eliminated by flow cytometry (BD FACSAria III; BD Biosciences, San Jose, CA).

The scRNAseq libraries were generated using Chromium Single Cell Next GEM 3′ Library & Gel Bead Kit v.3.1 (10x Genomics, Pleasanton, CA) according to the manufacturer's protocol. Briefly, cells were counted, diluted at 1000 cells/μL in PBS+ 0.04%, and 20,000 viable cells (10,200 for #756 mouse) were loaded in the 10x Chromium Controller to generate single-cell gel beads in emulsion. After reverse transcription, gel beads in emulsion were disrupted. Barcoded complementary DNA was isolated and amplified by PCR. Following fragmentation, end repair, and A-tailing, sample indexes were added during index PCR. The purified libraries were sequenced on a Novaseq (Illumina) with 28 cycles of read 1, 8 cycles of i7 index, and 91 cycles of read 2.

The sequencing reads of the Pb-PRL mice were demultiplexed and aligned to the human reference transcriptome (mm10-2020-A directly downloaded from 10x), using the Cell Ranger Pipeline software version 5.0.1 (10x

FLA 5.6.0 DTD ■ AJPA3976_proof ■ 22 October 2023 ■ 9:32 am ■ EO: AJPA-D-23-

Genomics). The unfiltered raw UMI counts from Cell Ranger were uploaded into Seurat software version 4.0.4[39] for quality control, data integration, and downstream analyses. The wild-type (WT) reads were downloaded from the GSE172515 Gene Expression Omnibus (GEO) repository[40] (*https://www.ncbi.nlm.nih.gov/geo/query/acc.cgi*, accession number GSE172515). Duplets, empty sequencing beads, and apoptotic cells were removed by filtering out cells with fewer than 500 features or a mitochondrial content higher than 20%.

Data from each sample were normalized and scaled using the log normalization method, and batch effect between samples was corrected using Seurat's FindIntegratedAnchors. On this integrated data set, the authors computed the principal component analysis on the 3000 most variable genes. UMAP was carried out using the 30 most significant principal components, and community detection was performed using the graph-based modularity-optimization Louvain algorithm from Seurat's FindClusters function. The human data set[30] is constituted by samples from the GSE172357 GEO repository[40] (*https://www.ncbi.nlm.nih.gov/geo/query/acc.cgi*, accession number GSE172357), and the filtered h5 files were processed in the same way as the mouse samples.

In Silico scRNAseq Analyses

scRNAseq data of vehicle-treated Pb-PRL mice (referred to as Pb-PRL mice in Figures 1, 2, and 3 for clarity) were compared with scRNAseq data sets of three WT mice (#1, #3, #7) from Joseph et al,[30] excluding urethral cells. Each sample was processed independently and then integrated together using the standard integration methods provided by Seurat. A total of 51,307 cells for the mouse data set (3 WT, 2 Pb-PRL−vehicle, 2 Pb-PRL−ATT), and 83,894 from the human data set[30] (11 samples from 3 healthy and 4 untreated BPH subjects) were retained after filtering, and all clusters were annotated using a list of manually curated gene markers.

Differential expression was performed on the different groups using the FindMarkers function of Seurat on the RNA assay with default parameters (Wilcoxon testing with Bonferroni correction). Only genes with adjusted $P < 0.05$ were selected as significant. The lists of differentially expressed genes were further divided into UP- and DOWN-regulated genes based on the avg_log2FC; avg_log2FC >0 for the UP-regulated genes and avg_log2FC <0 for the DOWN-regulated ones. Pathway enrichment analysis was performed using the FGSEA package[41] and gene set from the mouse collections of MsigDB.[42,43]

Signature scores were calculated from curated list of genes (LSC^{med} cells,[27] Club cells,[30] Hillock[30] cells, AR-up and AR-down signaling,[23] STAT5,[44] PRL reactome antioxidant (GSEA, *https://www.gsea-msigdb.org/gsea/msigdb/cards/REACTOME_PROLACTIN_RECEPTOR_SIGNALING*, last accessed August 20, 2023) (Supplemental Table S1) using the AddModuleScore_Ucell function from the R package Ucell.[45] For trajectory analyses (cell plasticity), the BAM files generated by Cell Ranger were processed independently using the velocyto software[46] with default parameters, and the resulting loom files were load, integrated, and then analyzed with scVelo.[47] The average velocity values associated to each cluster were then projected on the UMAP. scRNAseq data have been uploaded to the GEO repository (*https://www.ncbi.nlm.nih.gov/geo/query/acc.cgi*; accession number GSE235859).

Transcriptomic Analysis of Sorted Pb-PRL Epithelial Cells

Gene expression analysis of basal, LSC^{med}, and luminal cells sorted from Pb-PRL mice was performed using GeneChip Mouse Transcriptome Arrays 1.0 (Affymetrix, Santa Clara, CA), interrogating more than 6.0 million probes covering coding transcripts (70% of probes) and noncoding transcripts (30% of probes). The experiment was performed together with previously described analysis of cognate cell compartments from WT littermates [23]. Microarray data have been deposited on the ArrayExpress repository (BioStudies, *https://www.ebi.ac.uk/biostudies/studies/S-BSST1128*, last accessed September 13, 2023).

Organoid Assay

Mouse prostate basal and LSC^{med} cell populations were sorted based on their Lin/Sca-1/CD49f antigenic profile using BD FACSAria III (BD Biosciences) as previously described.[23,24,48] For organoid generation, the authors used the reference protocol described by Clevers' lab,[49] except that N-acetyl cysteine (NAC) was omitted in the culture medium. LSC^{med} and basal cells sorted from Pb-PRL mouse prostates were plated in triplicate (3000 cells/well) on a Low Growth Factor-containing Corning Matrigel (Sigma-Aldrich, Darmstadt, Germany) layer in a 96-well plate (Sarstedt, Nümbercht, Germany). After 1-day incubation, the medium was removed, and cells were covered by a new layer of Matrigel in order to perform 3-dimensional culture. After the second layer of Matrigel had solidified, 100 μL of fresh medium containing 10 μmol/L ATT (*versus* DMSO) were added to each well. The medium was changed every other day. After 10 days of Matrigel embedding, organoids were fixed in 4% PFA (Cat. No: 047377.9M; Thermo Fisher Scientific, Kandel, Germany), and photos were taken with a 4× objective under a M5000 EVOS inverted microscope in order to cover the entire surface of the well. Counting (number) and surfacing (size) were performed on QuPath software version 0.3.0 by manually surrounding the organoids.

Cell Lines

The BPH-1 prostate epithelial cell line (immortalized from a 68-year−old BPH patient using SV-40 T-antigen) was purchased in 2019 from DSMZ, German Collection of

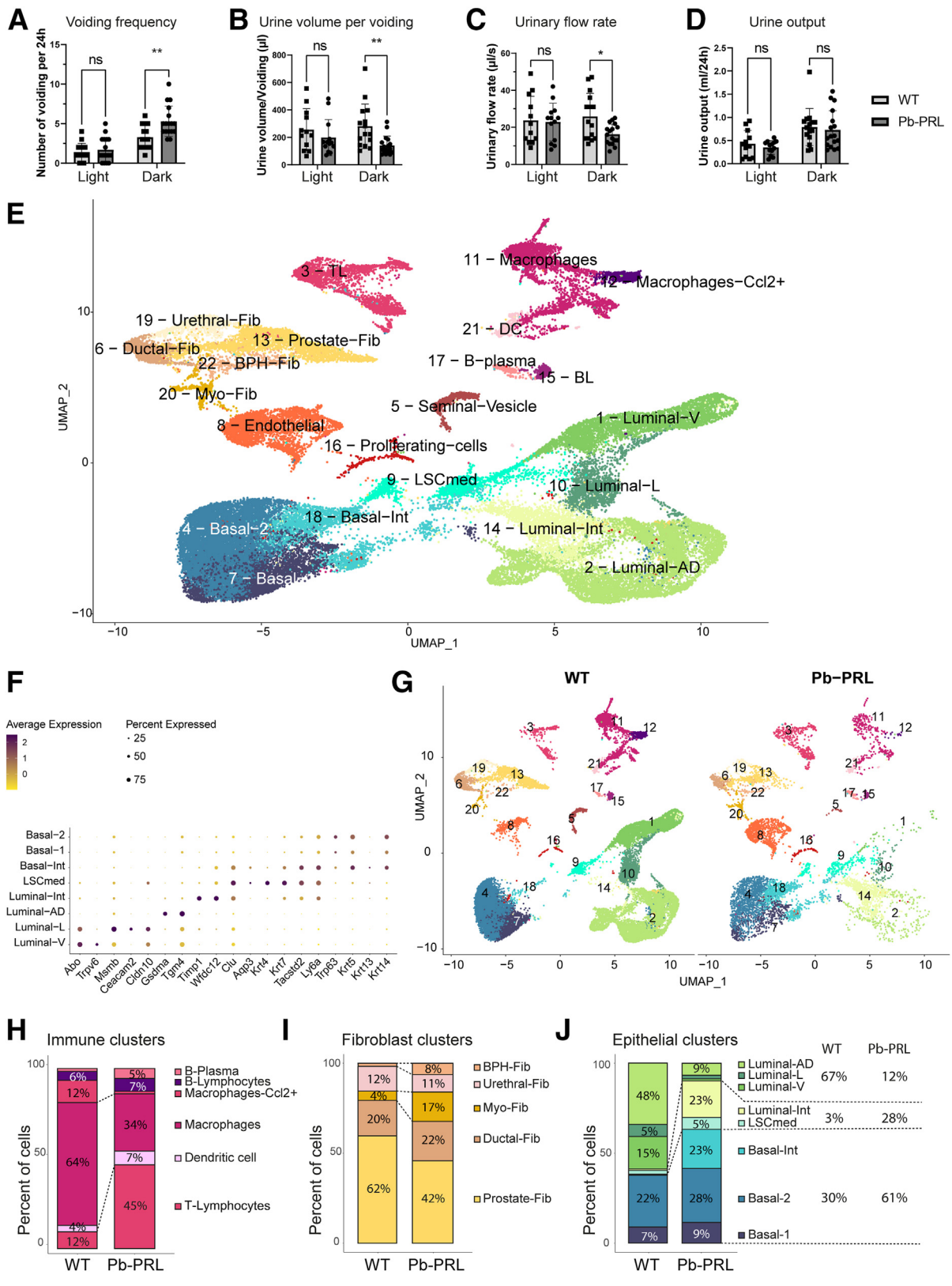

Figure 1 Pb-PRL mice exhibit marked alteration of urodynamic parameters and of prostate cell composition. **A**–**D:** Comparison of various urodynamic parameters (as indicated) between 15 wild-type (WT) and 17 Pb-PRL mice measured during light and dark periods. Error bars represent standard deviations. **E**–**J:** Single-cell RNA sequencing analyses of WT and Pb-PRL mouse prostates. **E:** UMAP of 51,307 single cells from the mouse data set after quality control. A resolution of 1.4 allows the identification of 22 cell types annotated based on the expression of 55 prostate genes, as shown in Supplemental Figure S3. **F:** Dot plot of the expression of the specific markers used to annotate the epithelial cell populations of the mouse data set. **G:** UMAP representation colored by the annotated cell type and split by the genotype (WT and Pb-PRL) (individual mice shown in Supplemental Figure S4A). **H**–**J:** Proportion of the cell type within

Microorganisms and Cell Cultures (Braunschweig, Germany; ACC 143, reference 1402). The WPMY-1 prostate myofibroblastic cell line (immortalized from a 54-year−old man using SV-40 T-antigen) was purchased in 2020 from ATCC (Manassas, USA; ATCC CRL-2854). Both cell lines were routinely maintained in Dulbecco's modified Eagle's medium (DMEM) medium (Glutamax, 4.5 g/L D-glucose + pyruvate, reference 31966-0.21; Gibco, Les Ulis, France) with 10% (BPH-1) or 5% (WPMY-1) fetal bovine serum (CVFSVF00-01; Eurobio Scientific, Les Ulis, France). Cells were passaged every 3 to 4 days.

Expression Array

Two million BPH-1 cells were seeded in a 100-mm Petri dish. Medium was replaced 24 hours after seeding, then fresh medium containing 10 μmol/L ATT or vehicle was added for 72 hours. Cells were trypsinized and centrifuged to dry; pellets were stored at −20°C. RNA was extracted using NucleoSpin (Macherey Nagel, Hoerd, France) according to the manufacturer's protocol and quantified using Nanodrop 2000 (Thermo Fischer Scientific). RNA quality was checked with BioAnalyser 2100 (Agilent Technologies, Les Ulis, France), then 5 μL of RNA at a concentration of 120 ng/μL were used for library generation. Clariom_S_Human arrays were used on the GeneChip 3000 7G scanner (Thermo Fisher Scientific). Results were processed with Transcriptome Analysis Console TAC4.0 (Thermo Fisher Scientific) and normalized with summarization methods RMA. Function pathways were determined using INGENUITY (Qiagen, Courtaboeuf, France) based on a differentially expressed gene list with fold-change 1.2 and $P = 0.05$ (529 genes). Heatmap was done using GraphPad Prism software version 9.3.1 (GraphPad Software, La Jolla, CA) and a list of differentially expressed genes with fold-change 2 and $P = 0.05$ under *t*-test (26 genes). Microarray data have been deposited on the ArrayExpress repository (BioStudies, *https://www.ebi.ac.uk/biostudies/studies/S-BSST1129*, last accessed September 13, 2023).

Live Cell Imaging

BPH-1 and WPMY-1 cells were seeded in 12-well plates at a density of 50,000 cells and 100,000 cells per well, respectively. Images (20×) of the same fields were taken every hour for 72 hours by a real-time IncuCyteS3 Live-Cell analysis system (Essen Bioscience). Confluence areas were analyzed using the IncuCyte software version 2022A, and results are displayed normalized to the initial time point (time t = 0).

Cell Numeration

BPH-1 cells were seeded in T75 flasks at the density of 35,000 cells. Fresh media containing ATT or vehicle was changed every 72 hours. Every 7 days, images of the flask were taken using phase contrast microscope (EVOS 5000; Thermo Fisher Scientific) before the cells and the medium were collected and counted using a Malassez cell chamber with Trypan blue.

Seahorse (OCR and ECAR)

BPH-1 and WPMY-1 cells were seeded in a specialized 96-well Seahorse XF96 V3 PS microplate (101085-004; Agilent Technologies) at the density of 1000 and 5000 cells per well, respectively. Seventy-two hours after ATT treatment, cells were incubated for 1 hour in unbuffered XF assay medium (Agilent Technologies) without ATT supplemented sequentially with either 2 mmol/L glutamine, 25 mmol/L glucose (G8769, Sigma-Aldrich), and 1 mmol/L sodium pyruvate for oxygen consumption rate (OCR) analysis, or 2 mmol/L glutamine for extracellular acidification rate (ECAR) analysis. XF Cell Mito Stress Test (103015100; Agilent Technologies) and XF Glycolysis Test assay (103020-100; Agilent Technologies) were used for OCR and ECAR measurement, respectively.

Compounds (all from Sigma-Aldrich) were injected during the assay at the following final concentrations. For OCR measurements: 1 μmol/L oligomycin (Ref. 75351, ATP synthase inhibitor); 0.5 μmol/L FCCP (Ref. 370-86-5, uncoupling agent measuring the maximal respiration capacity); 1 μmol/L antimycin A (Ref. A8674, mETC inhibitor); for ECAR measurements: 10 mmol/L glucose; 1 μmol/L oligomycin; 50 mmol/L 2-deoxyglucose (Ref. D6134, glycolytic inhibitor). Data were recorded using XFe 96 Extracellular Flux Analyzer (Agilent Technologies), normalized using protein concentration, and analyzed using Wave software version 2.6.3 (Agilent Technologies).

Extracellular Lactate and Glucose Measurement

BPH-1 and WPMY-1 cells were seeded in a 12-well plate at a density of 50,000 and 100,000 cells per well, respectively. After 30 minutes, 2 hours, 24 hours, 48 hours, and 72 hours after treatment, 200 μL of the medium of the corresponding wells were taken and put into a 96-well plate end rapidly stored at −20°C. The rest of the media was kept separate to determine protein concentration (Pierce BCA protein assay kit 23225; Thermo Fisher Scientific). Glucose and lactate media concentrations were measured with YSI 2090

the immune (**H**), fibroblast (**I**), and epithelial (**J**) cell populations between WT and Pb-PRL mice (bars color-coded according to panel **E**). Luminal-AD (luminal anterior/dorsal), Luminal-L (luminal lateral), and Luminal-V (luminal ventral) identify secretory luminal cells of the different lobes. $n = 7$ mice (**E** and **F**); $n = 3$ WT mice (**G**–**J**); $n = 2$ Pb-PRL mice (**G**–**J**). $^*P < 0.05$, $^{**}P < 0.01$ by two-way analysis of variance. Basal-Int, basal-intermediate; BL, B lymphocytes; DC, dendritic cells; Fib, XXX; luminal-Int, luminal intermediate; Myo, XXX; ns, not significant; TL, T lymphocytes.

FLA 5.6.0 DTD ■ AJPA3976_proof ■ 22 October 2023 ■ 9:32 am ■ EO: AJPA-D-23-

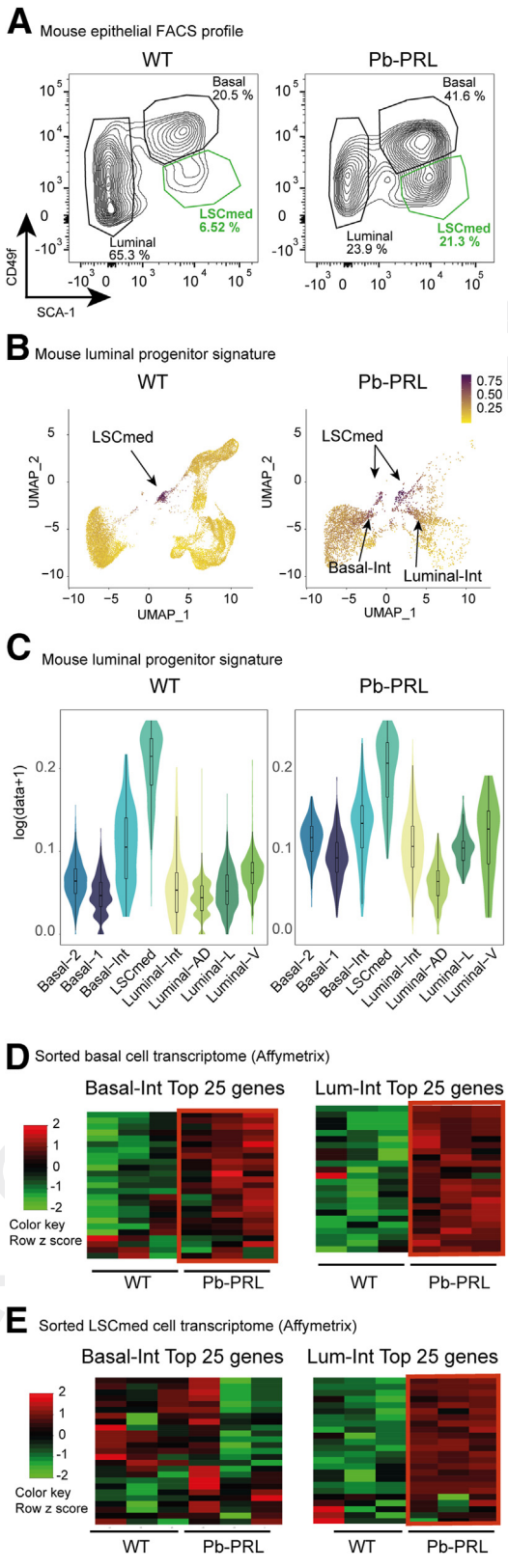

Figure 2 Cell sorting-scRNAseq correspondence of BPH-associated epithelial cell populations. **A:** Representative cell sorting prolife of wild-type (WT) and Pb-PRL mouse prostates using CD49f and SCA-1 cell markers. **B** and **C:** LSC^{med} cell location in the epithelial clusters for both WT and Pb-PRL genotypes shown as UMAP (**B**) and violin plots (**C**). Genes of the signature are listed in Supplemental Table S1. **D** and **E:** Enrichment of the top 25 genes of Basal-Int and Lum-Int clusters in the transcriptome of LSC^{med} (**D**) and basal (**E**) cells sorted from WT and Pb-PRL mice, as indicated. $n = 3$ WT mice; $n = 2$ Pb-PRL mice. AD, anterior/dorsal; Int, intermediate; L, lateral; V, ventral.

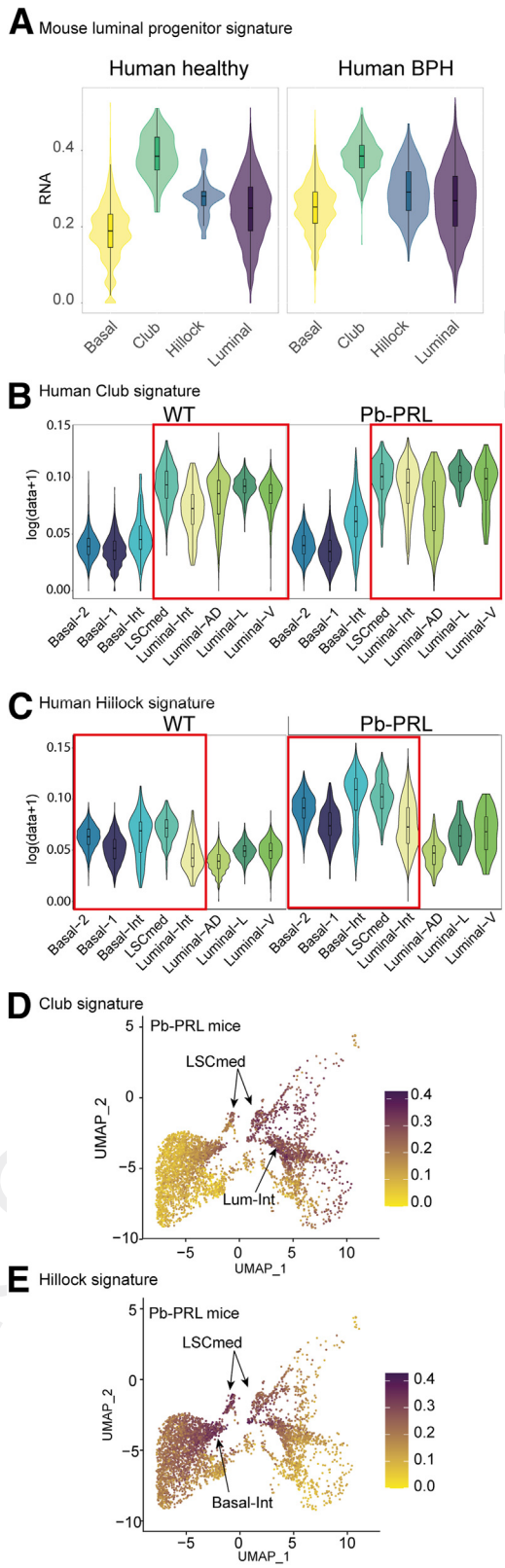

Figure 3 Mouse—human correspondence of BPH-associated epithelial cell populations. **A:** Violin plot of the epithelial compartment of human prostate (healthy and BPH) showing an enrichment of the LSC^{med} score in Hillock and Club cell clusters. **B**—**E:** Reciprocally, the Club (**B** and **D**) and Hillock (**C** and **E**) signatures were found to be enriched in LSC^{med}-positive cells of the Pb-PRL mouse prostate. Genes of the signatures are listed in Supplemental Table S1. AD, anterior/dorsal; Int, intermediate; L, lateral; V, ventral.

FLA 5.6.0 DTD ■ AJPA3976_proof ■ 22 October 2023 ■ 9:32 am ■ EO: AJPA-D-23-

Table 2 Antibodies for Immunohistochemistry

Proteins	Species dilution	Demasking	DAB	Clone, reference
Ki-67	Rabbit 1/150	20 minutes, 95°C	1 minute	SP6, RBK02705, Diagomics
KRT4	Rabbit 1/150	30 minutes, 95°C	30 seconds	2F9, bsm-52062R, Bioss Antibodies (Nanterre, France)
P-Stat5	Rabbit 1/300	20 minutes 90°C	10 minutes	C11C5, Cell Signaling Technology
Anti-rabbit	1/1000	30 minutes, room temperature	NA	BA-1400 Vector Laboratories

NA, not applicable.

Biochemistry analyzer and normalized to protein concentration in the medium.

Mitochondrial Parameters

BPH-1 and WPMY-1 cells were seeded in a 6-well plate at a density of 200,000 and 90,000 cells per well, respectively. After 72 hours of treatment, cells were detached with trypsin (0.05%, 25300054; Gibco), collected, and then stained with different probes (see below) for 20 to 45 minutes at 37°C following the manufacturer's protocol in DMEM media. After probe staining, dead cells were stained using 2.5 μg/mL of DAPI (D1306; Invitrogen, Villebon-sur-Yvette, France) in HBSS medium (14175-053; Gibco). Viable cell dye intensity was measured by flow cytometry using Fortessa (BD Biosciences). A minimum of 50,000 events were analyzed for each condition. Data were processed using BD FACSDiva software and analyzed using FlowJo software on a median fluorescence-level gate on live cells.

The probe concentrations were the following (all from Life Technologies, Courtaboeuf, France): 20 nmol/L MitoProbe TMRM (M20036), 50 nmol/L MitoTracker green (M7514), and 50 nmol/L MitoTracker CMXRos (M7512). TMRM-positive control for mitochondrial membrane depolarization was done by treating cells with 50 mmol/L CPPP (M20036; Life Technologies) for 10 minutes at 37°C before staining. Cell viability was measured by the percentage of cells incorporating the DAPI (D1306; Invitrogen).

ALDH Activity

BPH-1 cells were seeded in 6-well plates at a density of 45,000 cells per well. After 72 hours of ATT treatment, medium and cells were collected, and aldehyde dehydrogenase (ALDH) activity was measured using the Aldefluor kit (01700; StemCell Technologies, Saint-Egrève, France) according to manufacturer's protocol by recording median of fluorescence by flow cytometry using flow cytometer (Fortessa; BD Biosciences). In order to create the ALDH activity-positive gate, a sample of cells from each condition was treated separately with the ALDH activity inhibitor diethylaminobenzaldehyde (DEAB) to provide a negative control. A minimum of 50,000 events were analyzed for each condition. Data were processed using BD FACSDiva software and analyzed using FlowJo software on the percentage of ALDH-positive cells (Aldefluor).

Immunohistochemistry

Immunohistochemical analyses were performed using the antibodies listed in Table 2, with pH6 citrate buffer. Antibodies were revealed using Vectastain Elite ABC Peroxydase Standard kit (# PK-6100; Vector Laboratories, Les Ulis, France). Antibodies were diluted in antibody diluent (ZUC025-500 Zytomed; Diagomics, Blagnac, France) with 0.1% Triton for primary antibodies, and 2% horse serum (S-2000; Vector Laboratories) in PBS-Triton 0.1% for secondary antibody. Prostate tissue sections (hematoxylin and eosin stain or immunohistochemistry) were digitally scanned using a NanoZoomer-2.0 RT scanner (Hamamatsu Photonics, Massy, France) coupled to NDP.view2 software analysis beta version U12388-01 (Hamamatsu Photonics). For quantification of immunostaining, computer-assisted analysis of digital (scanned) images on whole prostates was performed using QuPath software version 0.3.0 (*https://qupath.github.io*). To quantify nuclear immunostaining (Ki-67, pSTAT5, AR) in the epithelium, first, the random forest tree for tissue recognition was used to delineate and only include the glandular areas in the analysis for each prostate lobe that had been manually surrounded and recognized by the software as objects. The positive cell detection command was then applied to each prostate lobe to discriminate DAB (3, 3'-diaminobenzidine) staining-positive (DAB+) versus staining-negative (DAB−) cells. The detection and export steps were fully automated using batch processing script. The index of proliferation (Ki-67$^+$) and of STAT5 and AR activation was calculated as the ratio of the number of positive versus total (positive + negative) nuclei counted in the epithelium. The whole procedure was validated by comparing the results obtained by Qu-Path−assisted versus manual counting.

Quantitative PCR

Total RNA was isolated from separate prostate lobes using the NucleoSpin RNA XS (Macherey Nagel, Hoerd, France) for mouse samples or NucleoSpin RNA (Macherey Nagel)

FLA 5.6.0 DTD ■ AJPA3976_proof ■ 22 October 2023 ■ 9:32 am ■ EO: AJPA-D-23-

Table 3 Primers for Quantitative RT-PCR

	Primer direction	Sequence
Mouse genes		
Actin	Forward	5′—GATGTATGAAGGCTTTGGTC—3′
	Reverse	5′—TGTGCACTTTTATTGGTCTC—3′
Gpx4	Forward	5′—TGGATAAGTACAGGGGTTTC—3′
	Reverse	5′—TAGCTGAGTGTAGTTTACGTC—3′
Sod1	Forward	5′—CACTCTAAGAAACATGGTGG—3′
	Reverse	5′—GATCACACGATCTTCAATGG—3′
Sod2	Forward	5′—CCATTTTCTGGACAAACCTG—3′
	Reverse	5′—GACCTTGCTCCTTATTGAAG—3′
Cat	Forward	5′—CTCCATCAGGTTTCTTTCTTG—3′
	Reverse	5′—CAACAGGAAGTTTTTGATG—3′
Nrf2	Forward	5′—TGATGGACTTGGAGTTGCC—3′
	Reverse	5′—TCAAACACTTCTCGACTTACTCC—3′
Ar	Forward	5′—GAGAGAGGCAGCTTGTGCAT—3′
	Reverse	5′—TACTGAATGACCGCCATCTG—3′
Human genes		
ACTIN	Forward	5′—AAGACCTGTACGCCAACACA—3′
	Reverse	5′—TGATCTCCTTCTGCATCCTG—3′
KRT4	Forward	5′—GTACAGAATGTCTGGAGAATG—3′
	Reverse	5′—TGGTAGAGATGATCTTGCTG—3′
PPARg1	Forward	5′—AAAGAAGCCGACACTAAACC—3′
	Reverse	5′—CTTCCATTACGGAGAGATCC—3′

for human prostate cell line samples, according to the manufacturer's instructions. RNA concentrations were measured using Nanodrop 2000 (Thermo Fisher Scientific). RNA (250 ng) was reverse transcribed using GoScript Reverse kit (A5001 for human samples, and A2791 for mouse samples; Promega, Charbonnières-les-Bains, France). The cDNAs, at a final dilution of 1/100 for mouse samples and 1/200 for human samples, were then subjected to real-time PCR amplification using gene-specific primers (Table 3) at a final concentration of 400 nmol/L and purchased from Sigma-Aldrich (KiCqStart SYBR green probe), except mouse *Nrf2* and *Ar* (Integrated DNA Technologies Europe, Leuven, Belgium), which were used at 1× final concentration. Real-time PCR was performed using Qtower software version 2.0 (Analytik Jena, Jena, Germany). The real-time quantitative PCR (qPCR) reaction contained 2 μL of cDNA sample (25 ng for mouse and 12.5 ng for human) and 10 μL of master mix with 1× GoTaq qPCR Master Mix (A6002; Promega) and 0.8 μL primer (10 μmol/L) and 7.2 μL of RNA/DNA-free water. Actin was used as housekeeping gene in each reaction. The Qtower 2.0 Instrument was used with the following program: enzyme activation: 95°C for 2 minutes; amplification (40 cycles): 95°C for 15 seconds, 60°C for 60 seconds. Results were generated with Qtower software version 2.0, and analyzed by the comparative cycle threshold method, and presented as fold change in gene expression relative to actin expression.

Western Blotting

Freshly trypsinized cells were centrifuged then dry pellets were snap-frozen in liquid nitrogen and stored at −20°C until processing. Cells were lysed with RIPA buffer (Handmade, NaCL 150 mmol/L, Tris 50 mmol/L pH 8, NP40 1%, SDS 0.1%, Na-deoxycholate 0.5%) with protease and phosphatase inhibitor cocktail (PPi 78445; Thermo Fisher Scientific). Protein concentrations were determined with Pierce BCA protein assay kit (23225; Thermo Fischer Scientific) using a density optic plate reader (ClarioSTAR, BMG Biotech, Champigny sur Marne, France). Equal protein concentrations (15 to 50 μg) were diluted and denatured in 4× Laemmli buffer (Nupage NP007; Invitrogen) with 2% of β-mercaptoethanol (M7522; Sigma-Aldrich) by heating at 95°C for 5 minutes. Proteins were resolved in 4% to 12% gradient SDS-PAGE in NuPAGE Bis-Tris Precast Gels (Life Technologies) with BlueStar PLUS Prestained protein marker (MWP04 Nippon Genetics Europe, Düren, Germany). Proteins were then transferred onto a 0.45-μm polyvinylidene difluoride membrane (IEVH85R Immobilon-E; Millipore, Guyancourt, France), and membranes were blocked with 5% nonfat dry milk with PBS-T (DPBS with 0.1% Tween-20) and stained with primary antibodies (Table 4) overnight at 4°C under agitation diluted as described below. For band detection, horseradish peroxidase—coupled secondary anti-rabbit (7074; Cell Signaling Technology, Leiden, Pays-Bas) or anti-mouse (NA931; GE Healthcare Europe, Freiburg, Germany) antibodies were added for 1 hour at room temperature under agitation before ECL substrate (Immobilon Western Chemiluminescent HRP Substrate WBKLS0500, or Immobilon Forte WBLUF0500, both from Millipore). Protein bands were visualized using ChemiDoc Imaging System (Bio-Rad Laboratories, Hercules, CA), and bands were quantified using

Table 4 Antibodies for Western Blotting

Antigen	Species dilution	Clone, reference
GAPDH	Mouse 1/1000 in nonfat milk 5%	Sc-47324, Santa Cruz Biotechnology (Heidelberg, Germany)
P21	Mouse 1/1000 in nonfat milk 5%	Sc-6246, Santa Cruz Biotechnology
PPARγ	Rabbit 1/1000 in BSA %	C26H12, Cell Signaling Technology
FABP4	Rabbit 1/1000 in nonfat milk 5%	2120S, Cell Signaling Technology
MDA	Mouse 1/1000 in BSA 5%	Ab-243066, 11E3, Abcam (Paris, France)
Anti-rabbit	1/10,000 in nonfat milk 5%	7074S, Cell Signaling Technology
Anti-mouse	1/10,000 in nonfat milk 5%	7076S, Cell Signaling Technology

BSA, bovine serum albumin.

Image Lab Software (Bio-Rad Laboratories). Staining intensities were normalized on GAPDH staining.

Statistics and Reproducibility

Statistical analyses were done using GraphPad Prism software version 9.3.1. Data are presented as means ± SD, or as ratio (ATT versus vehicle, Pb-PRL versus WT) as indicated. Wilcoxon test was used for urodynamic tests comparing the same mice before and after treatment, otherwise Mann-Whitney or analysis of variance was used for other mouse data, and *t*-test or analysis of variance was used for BPH-1 cell data.

Results

Pb-PRL Mice Exhibit Urodynamic Disturbances

The previously reported BPH hallmarks harbored by Pb-PRL mice have been widely documented[15,17–22] and are summarized in Supplemental Figure S1. To further assess the relevance of Pb-PRL mice as a BPH model, the authors analyzed various urodynamic parameters of Pb-PRL versus WT mice using metabolic cages. As expected, values for voiding frequency, urine output, and water intake were greater in the dark than in the light period for both genotypes ($P < 0.05$, two-way analysis of variance), and no genotype-related difference in any parameters could be observed in the light period (Figure 1, A–D, and Supplemental Figure S2). In the dark period, voiding frequency was significantly higher in Pb-PRL than in WT mice 5.29 ± 1.93 vs. 3.27 ± 1.49, $P = 0.0010$) (Figure 1A), whereas urine volume per voiding (140.8 ± 68.4 μL vs. 280.3 ± 162.7 μL, $P = 0.0080$) (Figure 1B) and urinary flow rate (16.2 ± 5.5 μL/second vs. 25.9 ± 12.5 μL/second, $P = 0.0239$) (Figure 1C) were concomitantly decreased in Pb-PRL mice. The urine output (diuresis) (Figure 1D), mean micturition duration, and water intake (Supplemental Figure S2, B and C) were similar for both genotypes. Together, these experiments assess that Pb-PRL mice exhibit urodynamic disturbances reminiscent of LUTS observed in patients with BPH.

Single-Cell Analysis of Pb-PRL Mouse Prostates

To address the cellular and molecular alterations underlying the various BPH hallmarks of Pb-PRL mice, we collected droplet-based scRNAseq profiles from 24,721 live cells originating the four prostate lobes of four Pb-PRL mice (Table 1). These data were analyzed together with publicly available data sets of three WT mouse prostates from which urethral cells had been excluded.[30] Unsupervised clustering segregated 22 distinct cell subsets that were annotated using marker genes validated for the mouse prostate[40,50–53] (Supplemental Figure S3). These markers identified eight epithelial, six immune, five stromal, one endothelial, one seminal vesicle, and one proliferating cell clusters (Figure 1, E–G, and Supplemental Figure S4A).

Pathway enrichment analysis in epithelial, immune, and stromal cell compartments identified TNFα/NFκB, hypoxia, and apoptosis/cell death in the top 20 pathways activated in all of them (Supplemental Figure S5 and Supplemental Table S2). Compartment-specific pathways included cell differentiation (development, epithelial-to-mesenchymal transition, wound healing) in the epithelium, and inflammatory pathways in stromal (inflammatory response, IL-6/STAT3) and immune (inflammatory response, IL-2/STAT5, interferon) cell compartments. In agreement with histopathological characterizations,[15,21] immune cells infiltrating Pb-PRL mouse prostates mainly involved T lymphocytes and macrophages, whereas the latter dominated the rare prostate-resident immune cells found in WT mouse prostates (Figure 1H). In the stroma, the main alterations in Pb-PRL mice were the decreased ratio of the prostate-fibroblast cluster to the benefit of myofibroblasts (in agreement with increased Picrosirius Red staining, Supplemental Figure S1F), and of a cluster of prostate fibroblasts enriched in *Egr1*, *Junb*, and *Sox10*. This cluster was named BPH-Fib because it was virtually absent in healthy prostate (Figure 1I).

The epithelial compartment of Pb-PRL prostates was more strongly affected (Figure 1, F, G, and J). The basal cell compartment was composed of three clusters. Basal 1 and Basal 2 clusters were transcriptionally similar and found at similar prevalence in both genotypes. The third cluster was virtually absent in healthy prostates but represented approximately 20% of the Pb-PRL prostate epithelium (Figure 1J). This cluster hereafter referred to as "Basal-Int" (for "intermediate" between the basal and luminal lineages) was characterized by high expression of *Krt13*, a marker of Hillock cells in the human prostate,[29] and *Tacstd2* (encoding TROP2) and *Ly6a* (encoding SCA-1), two typical stemness genes. The luminal secretory cell compartment was markedly reduced in Pb-PRL mice (from >60% to <20%) to the benefit of two clusters of nonsecretory luminal cells referred to as LSC^{med} and luminal-intermediate (Lum-Int) (Figure 1J, and Supplemental Figure S4B). Typical markers of LSC^{med} cells include *Krt4*, *Krt7*, *Clu*, and *Psca*,[23] whereas Lum-Int cells are characterized by *Pate6*, *Wfdc12*, and *Timp1* and low levels of secretory luminal cell markers (Figure 1F).

Overall, this scRNAseq analysis indicated that the epithelium of Pb-PRL prostate is much more heterogeneous than in healthy prostate, reminiscent of what has been observed in the human prostate from old donors, including BPH, versus young donors.[30,31] We therefore focused our study on the epithelial compartment.

Characterization of BPH-Associated Epithelial Cell Clusters

LSC^{med} defines a population of SCA-1^{+} luminal cells that can be enriched from mouse prostate by SCA-1/CD49f cell sorting

FLA 5.6.0 DTD ■ AJPA3976_proof ■ 22 October 2023 ■ 9:32 am ■ EO: AJPA-D-23-

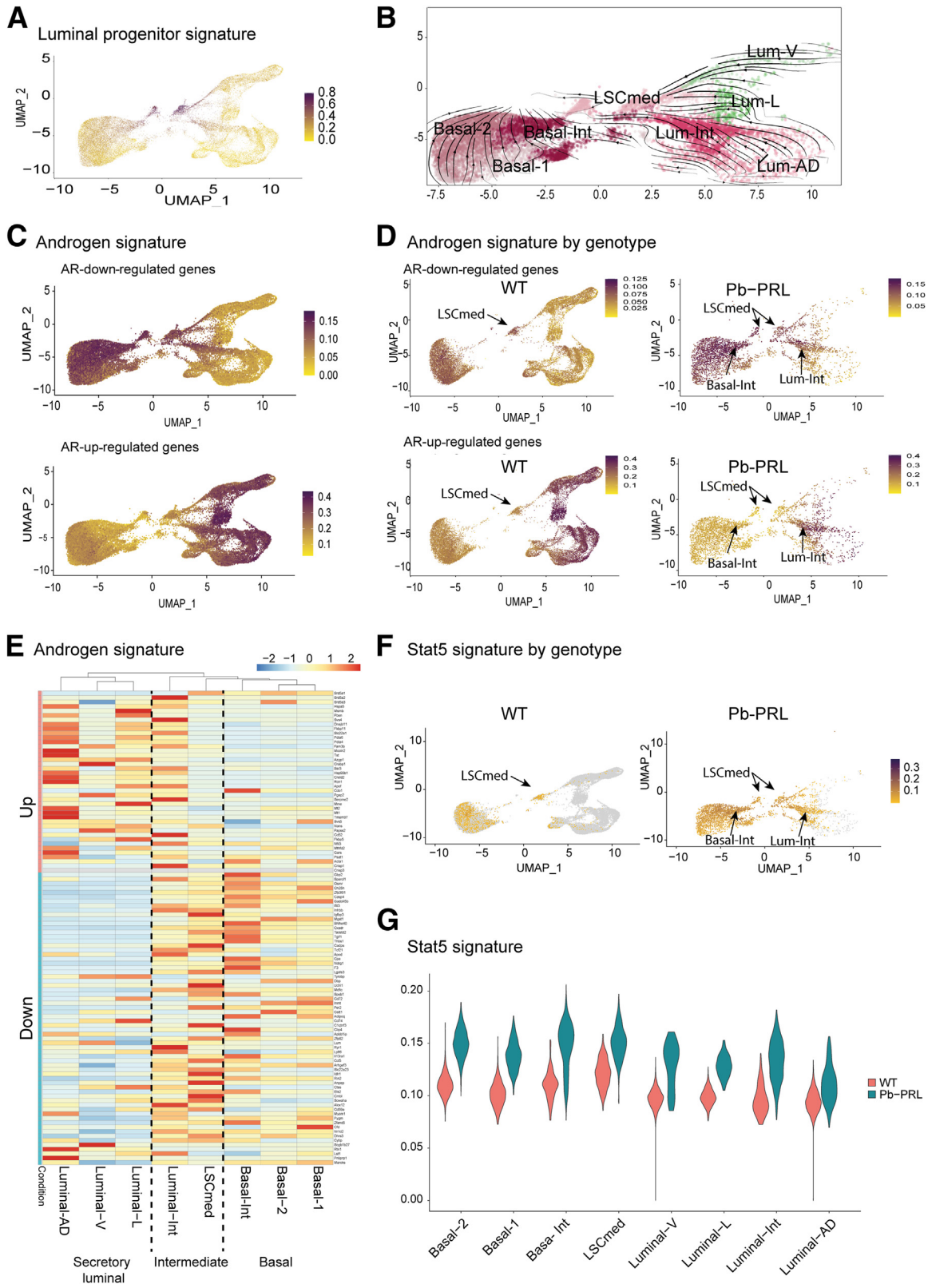

Figure 4 BPH-associated epithelial cell clusters overlap with altered androgen and STAT5 signaling. **A:** LSC^{med} signature score in the epithelium of the mouse data set. **B:** The velocity vector field displayed as streamlines of the epithelial population in mice, showing the central role of LSC^{med}-positive cells in the epithelial plasticity. **C:** Up-regulation of AR signaling (bottom) is found in luminal cells, whereas AR down-regulation (top) characterizes basal cells (all mice). **D:** Same as in **C** shown per genotype (WT and Pb-PRL). **E:** Heatmap of the pseudo-bulk expression of the regulators of the androgen genes. Hierarchical clustering of the clusters was computed with a Pearson's correlation as a distance, and the genes were grouped in UP and DOWN based on AR-mediated regulation of their transcription. **F** and **G:** Level of STAT5 signaling in the different genotypes, visualized as UMAP (**F**) and violin plot (**G**) in wild-type (WT) versus Pb-PRL mice. Genes of the signatures are listed in Supplemental Table S1. $n = 7$ mice (**A**); $n = 3$ WT mice (**D**, **F**, and **G**); $n = 2$ Pb-PRL mice (**D**, **F**, and **G**). AD, anterior/dorsal; Int, intermediate; L, lateral; V, ventral.

(Figure 2A).[23,24] This population was shown to largely correspond to the luminal progenitor cluster identified by scRNA-seq, from which a common signature of 15 genes was established[27,28] (Supplemental Table S1). In WT mice, this LSC^{med}/luminal progenitor signature marked a small scRNAseq cluster corresponding to the approximately 5% of epithelial cells enriched by cell sorting (Figure 2A) and was logically named LSC^{med} (Figure 2B). In Pb-PRL prostates, the luminal progenitor signature marked a second group of cells identified as part of the LSC^{med} cluster (Figure 2B). In addition, there was a global trend for the enrichment of LSC^{med} genes in contiguous Lum-Int and Basal-Int clusters (Figure 2, B and C). Enrichment analysis of the top 25 genes of these two clusters in the transcriptomes of FACS-sorted LSC^{med} and basal cell populations (BioStudies, *https://www.ebi.ac.uk/biostudies/studies/S-BSST1128*, last accessed September 13, 2023) suggested that, in Pb-PRL mice, Basal-Int cells preferentially segregate with basal cells, whereas Lum-Int cells segregate with both sorted LSC^{med} and basal cells (Figure 2, D and E). These data support that the enrichment of basal and LSC^{med} cells observed in sorting profiles of Pb-PRL prostates (Figure 2A) is due, at least in part, to the cosegregation of disease-associated Basal-Int and Lum-Int cells.

In agreement with the authors' former reports,[27,28] the mouse luminal progenitor signature was enriched in Club and Hillock cells of the human prostate, especially in BPH-associated Club cells (Figure 3A and Supplemental Figure S6). Reciprocally, the human Hillock and Club signatures (Supplemental Table S1) were enriched in mouse LSC^{med} cells (Figure 3, B–E). More globally, both signatures were enriched in Pb-PRL prostates, on the basal side (including Basal-Int) for the Hillock signature (Figure 3, C and E), and on the luminal side (including Lum-Int) for the Club signature (Figure 3, B and D). Together, these data assess that Pb-PRL mouse prostates are enriched in features of cells that have been associated with human prostate aging and pathogenesis.[30,31]

BPH-Associated Epithelial Clusters Overlap Altered Androgen and STAT5 Signaling

The overlap of the LSC^{med} signature with the cell continuum linking basal and luminal cell clusters in Pb-PRL prostates (Figure 2B and Figure 4A) led the authors to investigate possible trajectories between them. As shown in Figure 4B (whole prostate shown in Supplemental Figure S7A), scVelo analysis proposed trajectories connecting secretory luminal cells to the LSC^{med} cluster, directly and/or through Lum-Int cells. In the basal compartment, the Basal-Int cluster was connected to the LSC^{med} compartment as well as to Basal 1 and Basal 2 clusters. This analysis indicates that cells enriched in LSC^{med} genes may act as a central hub integrating various transitional cell states in diseased Pb-PRL prostates. This behavior was also suggested by the gradient of expression of some cluster-specific genes (Supplemental Figure S7B).

Androgen signaling down-regulation has been shown to induce prostatic epithelial cell plasticity in WT mice.[50] In line with this, expression of *Ar* and 5α-reductase was decreased in Pb-PRL prostate tissue (Supplemental Figure S8, A–C). Androgens regulate target genes both positively and negatively.[53] Both signatures expectedly displayed a mirror image with up-regulated genes mainly expressed in the luminal cell compartment, and down-regulated genes mainly expressed in the basal compartment (Figure 4, C and D). LSC^{med} cells have intrinsically low androgen signaling.[23] Lum-Int cells exhibited a pattern halfway between LSC^{med} and luminal cells (Figure 4E), further supporting they constitute a hinge in the epithelial cell continuum of Pb-PRL prostates. In addition to these cell-specific profiles, androgen signaling was globally decreased in Pb-PRL compared with WT prostate epithelium as highlighted by the higher level of AR-repressed genes in Pb-PRL versus WT prostates (Supplemental Figure S8D). This was not due only to the enrichment in low androgen-signaling cells (Basal-Int, LSC^{med}, Lum-Int) at the expense of high androgen-signaling cells (secretory luminal), but also to reduced androgen signaling in cognate cell compartments, eg, basal and LSC^{med} clusters (Figure 4D and Supplemental Figure S8D).

Cell-autonomous JAK/STAT signaling has also been shown to regulate prostatic epithelial cell plasticity in inflammatory context.[54] STAT5 is the canonical PRLR signaling pathway in the prostate.[17,22] In WT mice, the PRLR reactome (including *Prlr*) was highly expressed in the luminal epithelium, but in the absence of local PRL expression, no STAT5 signaling was detected[22,24] (Figure 4, F and G, and Supplemental Figure S9). In Pb-PRL mice, PRLR/STAT5 signaling is triggered in the luminal epithelium by locally produced PRL (Figure 4F). The shift of PRLR reactome expression from luminal cells in WT prostates, to Lum-Int cells in Pb-PRL mice (Supplemental Figure S9, B and C), suggests a functional role of PRLR/STAT5 signaling in epithelial cell reprogramming in this BPH model. Of note, based on *Prlr* and PRLR reactome expression pattern, STAT5 signaling detected in the basal compartment in both genotypes is most likely triggered by other cytokines than PRL.

Together, the almost superimposable pattern of LSC^{med}, AR-repressed and STAT5 signatures strongly suggests the contribution of these two pathways to the emergence of intermediate/LSC^{med} cells in Pb-PRL prostates.

Pb-PRL Mice Are Responsive to Antioxidant Therapy

Like in human BPH, Pb-PRL mouse prostates displayed features of oxidative stress as the level of expression of antioxidant enzymes was uniformly decreased in Pb-PRL mice compared to WT animals (Figure 4, A and H). This was confirmed by RT-qPCR analysis of key antioxidant enzymes including the chief transcription factor *Nrf2*, *Gpx4*, *Sod1*, *Sod2*, and *Cat* (Figure 5B). Thus, the Pb-PRL model

FLA 5.6.0 DTD ■ AJPA3976_proof ■ 22 October 2023 ■ 9:32 am ■ EO: AJPA-D-23-

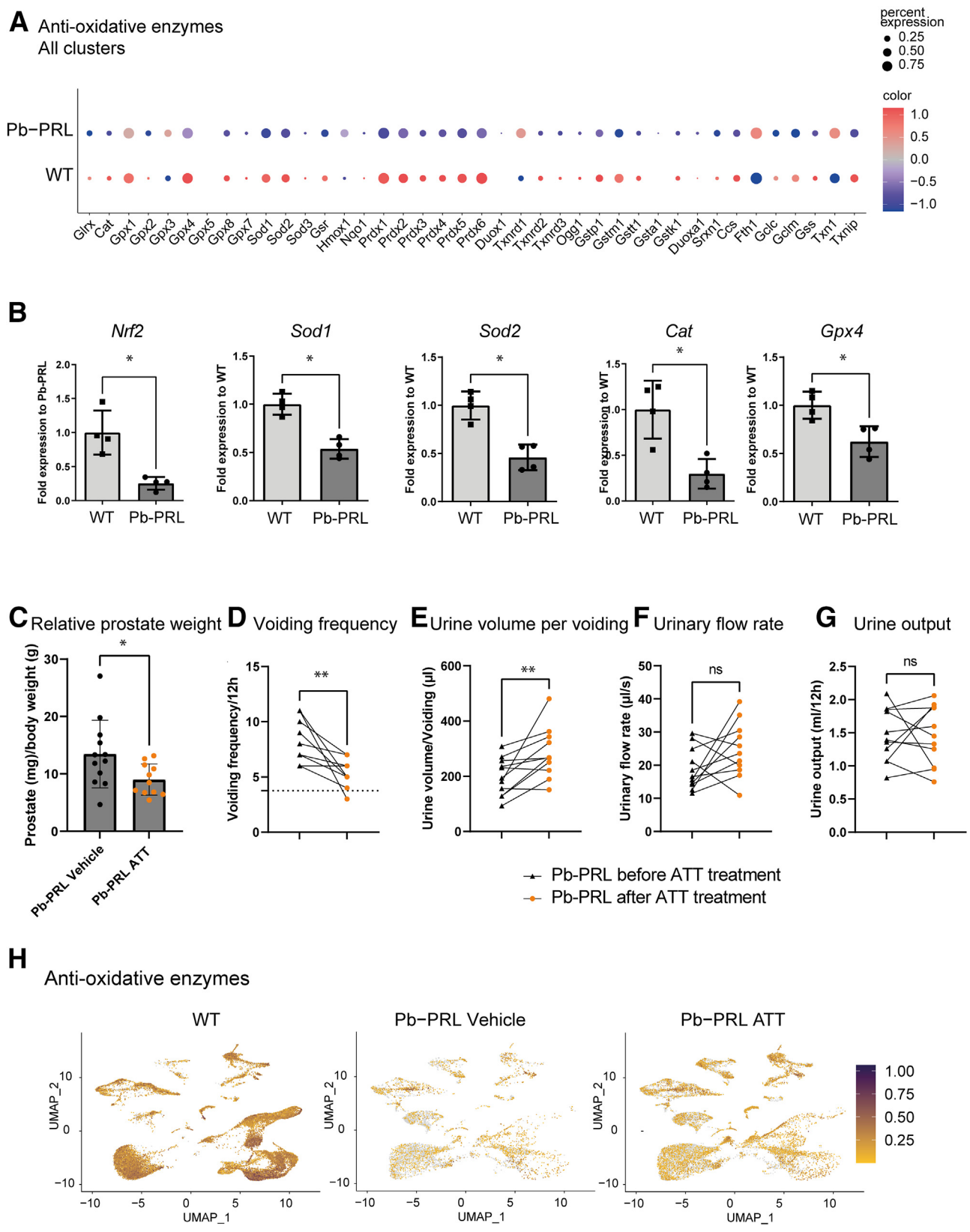

Figure 5 Pb-PRL mice are responsive to anethol trithione (ATT) therapy. **A:** The comparison of the expression of the anti-oxidative enzymes between wild-type (WT) and Pb-PRL mice highlights a decrease in overall expression in Pb-PRL mice. **B:** RT-qPCR analysis of selected anti-oxidative enzymes (*Gpx4*, *Sod1*, *Sod2*, *Cat*) and transcription factor (*Nrf2*) expressed in ventral prostates of Pb-PRL versus WT untreated mice (data normalized to WT). Error bars represent standard deviations. **C:** Prostate (mg)/mouse (g) weight ratio in Pb-PRL mice after 1-month ATT versus vehicle treatment. Error bars represent standard deviations. **D**–**G:** Evolution of various urodynamic parameters (as indicated) of Pb-PRL mice measured during the dark period before (baseline) versus after

was appropriate to investigate the potential benefit of antioxidant therapy in BPH.

ATT, a drug marketed in several countries for its choleretic and syalogogic properties,[55] is a specific inhibitor of reactive oxygen species (ROS) production at the Iq site of the mitochondrial respiratory chain. As such, it is assumed to preserve mitochondria activity and integrity in contrast to unspecific antioxidant molecules acting as ROS scavenger.[56] As shown in Figure 5C, 1 month of daily ATT treatment of Pb-PRL mice led to a significant decrease of prostate weight, but not of urinary bladder and urethral tissue weight (Supplemental Figure S10A). Compared with pretreatment values, chronic antioxidant treatment resulted, in the dark period, in significant reduction in voiding frequency and concomitant increase in urine volume per voiding, and in a trend (8 of 11 mice) to increased urinary flow rate (Figure 5, D–G). ATT had no effect on micturition duration and urine output, and vehicle failed to affect any parameter (Supplemental Figure S10B). Together, these data demonstrate the therapeutic benefit of antioxidant therapy in this model.

The histology of Pb-PRL prostates did not show any sign of marked alteration after ATT treatment (Supplemental Figure S11A). Also, STAT5 and AR signaling were not much affected by the treatment. At best, nuclear pSTAT5 immunostaining was slightly decreased in the epithelium of anterior and dorsal lobes (ie, the two lobes where it is the most highly activated in Pb-PRL mouse prostates) but it remained at such a high level that the STAT5 signaling signature was not impacted (Supplemental Figure S11, B–D). Similarly, both up and down AR signaling signatures were unchanged. In agreement, nuclear AR immunostaining in the epithelium, earlier shown to be of lower intensity in Pb-PRL versus WT mice,[23] was unaffected by ATT treatment (Supplemental Figure S11, E–G). Single-cell RNAseq analysis of prostates from vehicle- versus ATT-treated Pb-PRL mice showed only mild changes in cluster distribution, at best a slight decrease in the prevalence of disease-associated clusters Lum-Int, Basal-Int, and myofibroblasts could be observed (Supplemental Figure S12). Noticeably, the expression pattern of antioxidant enzymes was partially restored under ATT treatment (Figure 5H), including in epithelial cells.

ATT Reduces Proliferation and Mitochondrial Metabolism of BPH-1 Cells

The authors then used the BPH-1 cell line to investigate the effect of ATT on BPH epithelial cells.[57] Based on its keratin profile[57] this cell line has been described as luminal.[57] Its androgen insensitivity conjugated to the expression of typical luminal progenitor cell markers such as *KRT7*[57] and *KRT4* (Figure 6A), suggests it can be used as a model of [F6] LSC^{med}/Club-like cells. After 60 hours ATT treatment, a decrease in cell confluence was observed by IncuCyte analysis without alteration of cell viability (Figure 6, B and C, and Supplemental Figure S13A). This effect was concomitant to increase in p21 protein levels (Figure 6, D and E) and persisted over 3 weeks of chronic ATT treatment (Figure 6F and Supplemental Figure S13B).

ATT treatment has been shown to decrease mitochondrial ROS production on isolated rat heart mitochondria.[56] In BPH-1 cells, ATT reduced the level of malondialdehyde, a marker of oxidative stress (Figure 6, D and G). The authors hypothesized that the reduction of cell growth under ATT treatment could be related to cell metabolism impairment. After 72 hours of treatment, a decrease in mitochondrial activity measured by flow cytometry was observed (Figure 6H). This was confirmed by a significant decrease in mitochondrial respiration measured by OCR using Seahorse BioAnalyser: basal mitochondrial respiration, maximal respiration, and ATP production were all down-regulated (Figure 6, I and J). ATT treatment affected neither mitochondrial membrane potential nor mitochondrial mass (Figure 6, K and L). BPH-1 cells did not compensate the decrease in mitochondrial activity by up-regulating glycolysis, as the extracellular acidification rate remained similar between control and treated cells (Figure 6, M and N). The lack of glycolysis alteration by ATT treatment was also confirmed by measuring the extracellular lactate/glucose concentration ratio (Figure 6O).

Similar assays performed using the human myofibroblastic WPMY-1 cell line showed that ATT also affected the mitochondrial respiration (OCR) in this cell type, with a significant effect on mitochondrial membrane potential and a trend toward reduction of mitochondrial mass and activity (Supplemental Figure S14, A–E). ATT-induced accumulation of lactate in culture medium was observed from 48 hours of treatment (Supplemental Figure S14F), which may explain why it was not observed in short-term seahorse experiments performed in fresh medium (Supplemental Figure S14, G and H). These data may suggest mild up-regulation of glycolysis under ATT, which could explain the absence of impact on WPMY-1 cell proliferation (Supplemental Figure S14, I and J).

Together, these data suggest that ATT affects mitochondrial metabolism in both epithelial and myofibroblastic prostate cell lines, with different outcomes on cell proliferation depending on compensatory up-regulation of glycolysis.

1-month ATT treatment. See Supplemental Figure S10 for vehicle treatment. **Dotted line** in **D** represents averaged voiding frequency in 6-month–old WT mice. **H:** UMAP representation of antioxidative enzyme expression split by genotype and treatment (WT, Pb-PRL Vehicle, and Pb-PRL ATT). Genes of the antioxidant signature are listed in Supplemental Table S1. $n = 3$ WT mice (**A** and **H**); $n = 2$ Pb-PRL mice (**A**); $n = 4$ WT mice (**B**); $n = 4$ Pb-PRL mice (**B**); $n = 2$ Pb-PRL vehicle-treated mice (**H**); $n = 2$ Pb-PRL ATT-treated mice (**H**). $^{*}P < 0.05$ by *t*-test (**B**) or Mann-Whitney test (**C**), $^{**}P < 0.01$ by Wilcoxon test (**D**–**G**). ns, not significant.

FLA 5.6.0 DTD ■ AJPA3976_proof ■ 22 October 2023 ■ 9:32 am ■ EO: AJPA-D-23-

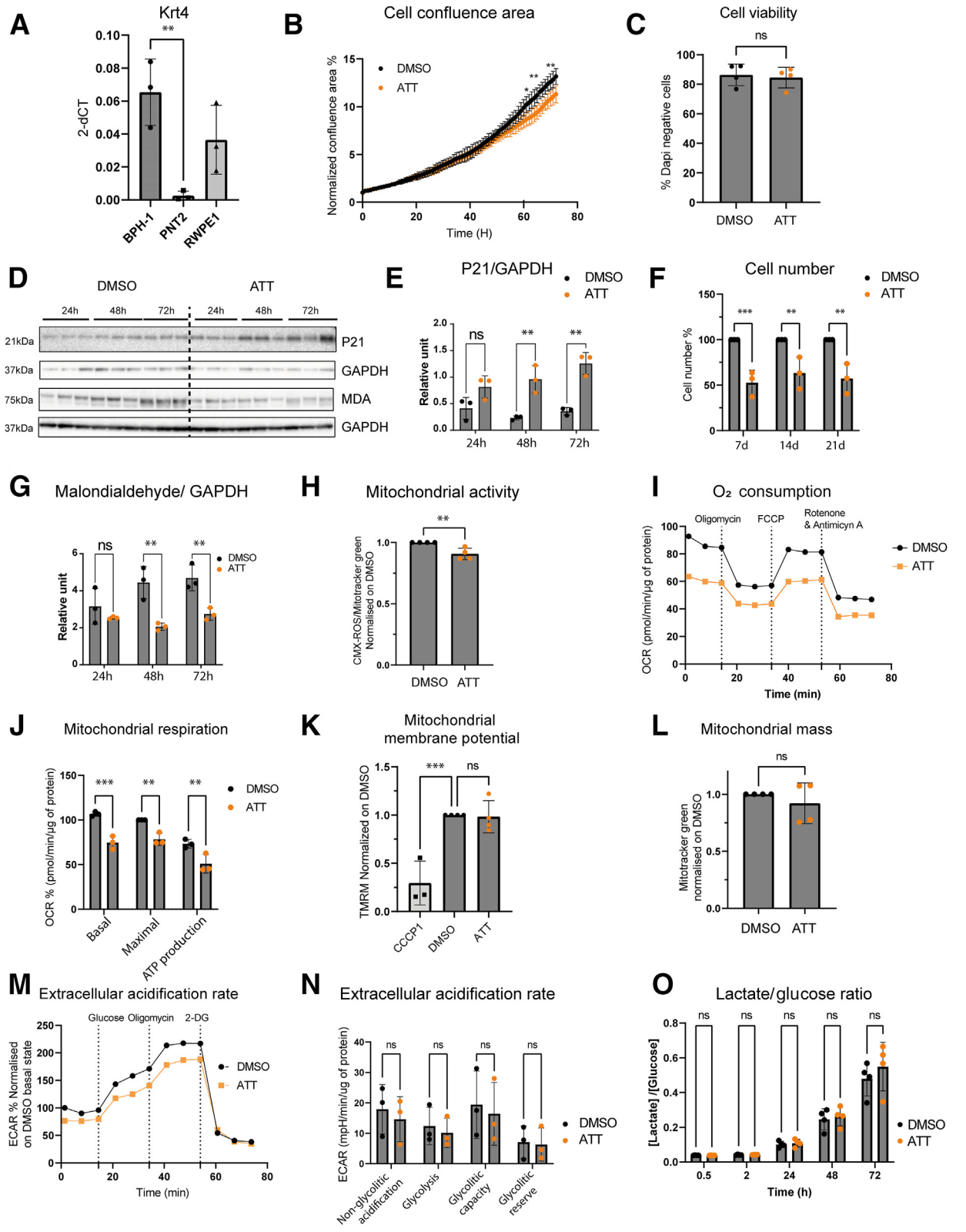

Figure 6 Anethol trithione (ATT) reduces oxidative stress, cell proliferation and mitochondrial metabolism in BPH-1 cells. **A:** mRNA expression of the LSC^{med} cell marker *KRT4* measured by RT-qPCR in three benign human prostatic epithelial cell lines: BPH-1 derived from a BPH patient, and PNT2 and RWPE1 derived from healthy donors. **B:** Mean cell confluence area in BPH-1 cells treated with 10 µmol/L ATT versus dimethyl sulfoxide (DMSO), normalized to day 0. Scans were acquired every hour for 72 hours using IncuCyte (see Supplemental Figure S11). **C:** Percentage of live BPH-1 cells treated for 72 hours with 10 µmol/L ATT versus DMSO measured by flow cytometry using DAPI. **D:** Immunoblot of P21, malondialdehyde (MDA), and for each, of GAPDH, after 24 hours, 48 hours, and 72 hours of treatment with 10 µmol/L ATT versus DMSO. The **dotted line** separates DMSO and ATT samples loaded on the same gel. **E:** Quantification

FLA 5.6.0 DTD ■ AJPA3976_proof ■ 22 October 2023 ■ 9:32 am ■ EO: AJPA-D-23-

print & web 4C/FPO

ATT Interferes with Progenitor Hallmarks of Epithelial Cells

Despite relatively mild transcriptomic effects, short-term (72 hours) treatment of BPH-1 cells with ATT affected various disease- and metabolism-related functions including free radical scavenging (Supplemental Figure S15, A–C). Strikingly, the most affected genes included markers of LSC^{med}/Club/Hillock cells (eg, *ALDH1A3*, *PPARG*, *KRT13*)[23,29,58,59] (Supplemental Figure S15D). In the prostate epithelium, *PPARG* is mainly expressed in luminal progenitor-like cells (mouse LSC^{med} and human Club/Hillock) (Figure 7A and Supplemental Figure S15, E and F), and mouse studies have suggested its involvement in epithelial cell differentiation.[60] *PPARG* expression in Club cells was increased in BPH versus healthy human prostate (Supplemental Figure S15F). The ATT-induced reduction of *PPARG* expression in BPH-1 cells was confirmed by RT-qPCR (Figure 7B) and immunoblot (PPARγ1 isoform), and the down-regulation of its transcriptomic target FABP4 assesses the functional down-regulation of this pathway by ATT (Figure 7, C and D).

ALDH1A3 is tightly correlated to cell stemness,[61] and high ALDH activity is a functional marker of mouse prostate stem/progenitor cells.[62] In the human prostate, *ALDH1A3* is expressed in luminal and Club/Hillock cells, and in the mouse, it is mostly expressed in disease-associated Basal-Int, LSC^{med}, and Lum-Int clusters (Figure 7E, and Supplemental Figure S15, E and F). In contrast to *ALDH1A3* expression measured by RT-qPCR (Figure 7F), treatment of BPH-1 cells by ATT drastically affected ALDH enzymatic activity as assessed in the Aldefluor assay (Figure 7, G and H).

The alteration of PPARγ and ALDH pathways suggested that ATT may interfere with the properties of progenitor-like cells. To address this hypothesis, the authors generated organoids from basal and LSC^{med} cells FACS-enriched from Pb-PRL prostates (Figure 7I). Although ATT treatment had mild (basal) or inconsistent (LSC^{med}) effect on organoid forming capacity (Figure 7J), a robust and highly significant inhibitory effect on organoid growth was noticed for both cell types (Figure 7K). Together, these data indicate that ATT impairs the growth of BPH-associated progenitor-like epithelial cells.

Discussion

Emerging evidence indicates that the prostate epithelium of the aging male, including the BPH condition, is progressively populated with luminal cells displaying low androgen signaling. Referred to as TROP2^{+} luminal cells in the mouse,[58,63] and CD38^{low} luminal cells[58,59] or Club cells[29–31] in humans, these cells largely overlap with LSC^{med} cells (for a review, see Baures et al[28]). As a consequence of their tolerance to low androgen conditions, these cells presumably contribute to therapeutic resistance as supported by the increased prevalence of LSC^{med} cells in castrated mice,[23,26,30,50] and of Club-like cells in 5-ARI–treated human BPH.[32] In both species, luminal cell reprograming into LSC^{med}/Club-like cells triggered by androgen signaling manipulation has been proposed as the underlying mechanism.[32,50] Is cell plasticity also driving LSC^{med}-like cell amplification during BPH pathogenesis? The identification of several intermediate cell states between luminal and basal lineages in Pb-PRL mouse prostates supports this hypothesis. In these mice, intraprostatic androgen signaling is decreased (this study) while STAT5 signaling is increased compared to WT mice.[19,22] *Stat5* knock-down in prostatic luminal cells of Pb-PRL mice reduces luminal cell depletion as well as other BPH hallmarks.[22] At the single-cell level, the present study shows that LSC^{med}, STAT,5 and AR-repressed gene signatures almost perfectly overlap, suggesting functional connections. Are these pathways also involved in human BPH pathogenesis? It is at present unknown. One can note, however, that circulating testosterone levels decline with age[64] when BPH and Club cell prevalence increases. Also, STAT5 signaling triggered by the inflammatory cytokine CCL5 has been proposed to promote BPH epithelial cell proliferation in low-androgen conditions.[65] Further studies are required to decipher the molecular circuitry integrating these pathways in BPH, including potential reciprocal regulation.

How could LSC^{med}/Club-like cells contribute to BPH pathogenesis? Beyond their survival advantage over luminal cells in low-androgen conditions, LSC^{med}-like cells are also more proliferative, exhibit higher organoid-forming capacity, and form larger prostaspheres and organoids.[24,26,28,58] These properties support their contribution to hyperplasia and hypertrophy of the periurethral (transition) prostate area

of P21 versus GAPDH proteins shown in **D**. **F:** BPH-1 cell numeration (Malassez cell) after 7, 14, and 21 days of chronic treatment with 10 μmol/L ATT versus DMSO (treatment renewed every 3 days). **G:** Quantification of malondialdehyde versus GAPDH proteins shown in **D**. **H**, **K**, and **L:** Relative median fluorescence intensity (MFI) measured by flow cytometry of CMXRos (**H**), TMRM (**K**) and MitoTracker Green (**L**) probes in BPH-1 cells after 72 hours of ATT (10 μmol/L) treatment. Each experiment is normalized to DMSO, and CMX-ROS MFI is also normalized to MitoTracker Green MFI. **I:** Representative BPH-1 cell O_2 consumption rate (OCR) after 72 hours of ATT (10 μmol/L) treatment measured by Seahorse. **J:** Quantification of OCR in BPH-1 cells after 72 hours of ATT (10 μmol/L) treatment, each point represents the mean OCR measured for 4 to 8 technical replicates and the maximal respiration is normalized to 100%. **M:** Representative BPH-1 cell extracellular acidification rate (ECAR) after 72 hours of ATT (10 μmol/L) treatment measured by Seahorse. Cells were incubated in fresh ATT-free Seahorse medium 1 hour before recording (T0). **N:** Quantification of ECAR in BPH-1 cells after 72 hours ATT (10 μmol/L) treatment, each point represents the mean of technical replicates. **O:** Ratio of extracellular lactate versus glucose concentration after 30 minutes, 2 hours, 24 hours, 48 hours, and 72 hours of ATT (10 μmol/L) treatment ($n = 4$). Each lactate and glucose concentration is normalized to the extracellular protein concentration. Error bars represent standard deviations. $n = 3$ experiments (**A**, **B**, **D**, and **J**); $n = 4$ experiments (**C**, **H**, **K**, **L**, and **O**); $n = 4$ to 8 technical replicates (**J**). $^{*}P < 0.05$, $^{**}P < 0.01$, and $^{***}P < 0.001$) by *t*-test (**A**, **C**, **H**, and **L**), one-way (**K**) or two-way analysis of variance (**B**, **E**, **F**, **G**, **J**, **N**, and **O**). ns, not significant.

FLA 5.6.0 DTD ■ AJPA3976_proof ■ 22 October 2023 ■ 9:32 am ■ EO: AJPA-D-23-

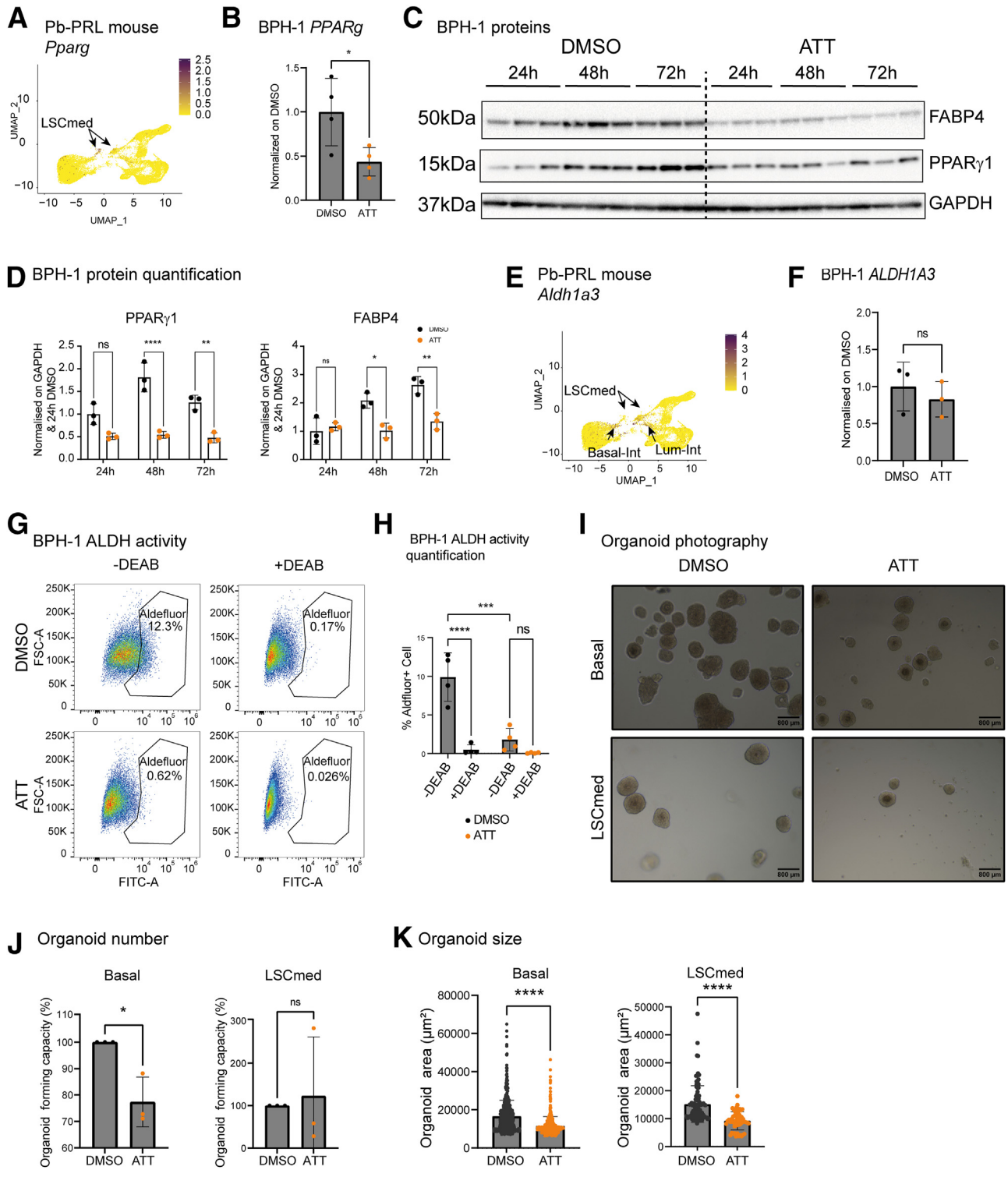

Figure 7 Anethol trithione (ATT) interferes with progenitor hallmarks of epithelial cells. **A**—**D:** Analysis of PPARg. **A:** Expression of *Pparg* in the epithelial subset of Pb-PRL—vehicle mice. **B:** mRNA expression of *Pparg* measured by RT-qPCR in BPH-1 cells treated for 72 hours with 10 µmol/L ATT versus dimethyl sulfoxide (DMSO). **C:** Immunoblot of PPARγ1, FABP4, and GAPDH proteins after 24 hours, 48 hours, and 72 hours of treatment with 10 µmol/L ATT versus DMSO (three independent samples shown). The dotted line separates DMSO and ATT samples loaded on the same gel. **D:** Quantification of PPARγ1/GAPDH and FABP4/GAPDH ratios normalized to the 24-hour DMSO condition. **E**—**H:** Analysis of ALDH1A3. **E:** Expression of *Aldh1a3* in the epithelial subset of Pb-PRL—vehicle mice. **F:** mRNA expression of *ALDH1A3* measured by RT-qPCR in BPH-1 cells treated for 72 hours with 10 µmol/L ATT versus DMSO. **G:** Representative experiment showing ALDH activity in BPH-1 cells after 72 hours of ATT versus DMSO treatment by flow cytometry using Aldefluor kit. DEAB is an ALDH activity inhibitor used to delineate the ALDH activity positive gate named Aldefluor. **H:** Percentage of Aldefluor-positive BPH-1 cells after 72 hours of treatment. Each point represents the mean of technical replicates. **I**—**K:** Organoid assay. **I:** Representative images of organoids derived from basal and LSC^{med} cell sorted from three non-treated Pb-PRL mice. Images were taken by light inverted microscope EVOS 5000 after 10-day treatment with ATT or DMSO. Treatments were started 1 day

ultimately leading to compression of the urethra. In this context, whereas 5-ARI treatment appears to favor Club-like cell expansion by cell plasticity, the identification of alternative therapeutic strategies targeting these cells (or luminal cell reprogramming) seems appropriate. This study shows that the antioxidant compound ATT prevented the growth of organoids generated from Pb-PRL LSC^{med} and basal cells, ie, the two epithelial cell compartments amplified in cell sorting (Figure 2A), as well as the proliferation of LSC^{med}-like human BPH-1 cells. These growth-inhibitory effects may result from reduced mitochondrial metabolism under ATT. Based on altered ALDH activity of BPH-1 cells and organoid-forming capacity of Pb-PRL basal cells, ATT may also affect the progenitor properties of BPH-associated cells. Importantly, 1-month antioxidant therapy with ATT reduced prostate weight and partly reversed the urodynamic disturbances exhibited by Pb-PRL mice. This is to our knowledge the first report showing that a drug affecting the growth of androgen-independent LSC^{med}-like cells also improves BPH symptoms *in vivo*. Given the wide panel of cells presumably affected by ATT, alternative mechanisms involving other cell compartments may also contribute to this therapeutic benefit.

Other antioxidant compounds have been recently reported as candidates for BPH therapy. These include mitoquinone, a mitochondria-targeted drug,[66] and apocynin, an NADPH oxidase inhibitor.[67] Both were shown to reduce cell proliferation, inflammatory hallmarks and prostate weight gain in a rat model of testosterone-induced prostate enlargement. No data, however, were provided on urodynamic parameters. Both compounds were shown to inhibit AR signaling, therefore one might predict that long-term therapy could ultimately increase the prevalence of androgen-independent Club-like cells by luminal cell plasticity, as observed with 5-ARI.[32] Such an outcome is not expected with ATT treatment. As mentioned, ATT has been used for decades as a treatment of xerostomia,[68,69] and it is well tolerated. Based on that data, we tentatively propose the following steps to validate ATT as a treatment for BPH. First, retrospective cohorts of patients treated with ATT for xerostomia should be analyzed to address the expected lower prevalence of urinary symptoms compared with the general population. This preliminary work should allow to collect specific data on these patients, including hydration habits (considering their xerostomia) as hydration can affect urinary symptoms. Second, a clinical trial should be developed to evaluate the efficacy of ATT in BPH treatment. Treatment-naive patients with symptomatic BPH should be randomized double-blind in two arms (ATT versus placebo), with improvement of urinary symptoms (International Prostate Symptom Score) as the primary endpoint. If ATT efficacy can be demonstrated, a comparative study involving ATT and α-blockers, the most widely used treatment worldwide, could then be proposed. As reported in former reference trials of BPH treatments,[5,6] such a study should benefit from long-term follow-up, including International Prostate Symptom Score and flow rate evaluation at 1 and 4 years. Secondary endpoints should include sexual side effects and patient satisfaction. A noninferiority trial compared with α-blockers would be sufficient, considering that side effects are lower with ATT (especially retrograde ejaculation). Finally, in light of these results showing that ATT alters the progenitor properties of androgen-independent cells, a similar trial involving 5-ARI instead of α-blockers may also be considered. In particular, it would be interesting to assess whether ATT could counteract the exhaustion of effect observed with long-term 5-ARI treatment, which we hypothesize to be causally related to the luminal-to−Club-like cell transition induced by the drug.[32] If so, such a drug combination may delay surgery in case of failure of 5-ARI treatment, with important socioeconomical impact.

This study faces some limitations. One major issue in the BPH field is the paucity of experimental models to address disease mechanisms and drug efficacy. BPH-1 is to our knowledge the only prostatic epithelial cell line generated from a BPH patient.[57] However, although its LSC^{med}-like features are appealing, the intrinsic features of this T antigen-immortalized cell line call for confirmation of experimental findings in more relevant models, eg, organoids generated from primary BPH cells. This issue is even more challenging for stromal cells, as we are not aware of any fibroblastic model generated from acknowledged BPH. This is the reason why we used the healthy, T antigen−immortalized WPMY-1 cell line to address the effects of ATT on myofibroblastic cells. Regarding *in vivo* studies, in contrast to prostate cancer for which the majority of preclinical research worldwide involves a few mouse models carrying the most frequent genetic alterations observed in patients,[70] there is currently no reference model for BPH. Indeed, many animal models of BPH models are difficult to handle, or even considered to be inconsistent with real state.[33] For example, although the above-mentioned testosterone-induced prostate enlargement rat model shows increased voiding frequency and reduced volume per voiding, it is known that in humans androgen levels decline in the elderly, when BPH prevalence increases.[71] In this context, former reports have shown that the histopathological alterations of Pb-PRL mouse prostates mirror human BPH.[15,17–22] This study provides additional evidence supporting the relevance of this mouse model: i)

after the cell seeding and renewed with fresh medium, every other day for 10 days. Quantification of the number of organoids (**J**) and organoid size (**K**) is shown. Each point in **K** represents a single organoid. Errors bars represent standard deviations. $n = 2$ mice (**A** and **E**); $n = 3$ mice (**I**); $n = 3$ experiments (**B**, **F**, and **I**); $n = 4$ technical replicates (**H**); $n = 4$ mice (**B** and **F**); $n = 4$ to 8 technical replicates (**J**). $^{*}P < 0.05$, $^{**}P < 0.01$, $^{***}P < 0.001$, and $^{****}P < 0.0001$ by *t*-test (**B**, **F**, and **J**), Mann-Whitney (**K**), or two-way analysis of variance (**D** and **H**). Scale bar = 800 μm. Original magnification, ×10 (**I**). ns, not significant.

FLA 5.6.0 DTD ■ AJPA3976_proof ■ 22 October 2023 ■ 9:32 am ■ EO: AJPA-D-23-

its micturition characteristics recapitulate the symptoms of urinary hesitancy and frequency seen in BPH patients; ii) their prostates present increased vulnerability to oxidative stress, as proposed in the human disease; and iii) their epithelium is heterogeneous and contains various Club/Hillock-like cell states exhibiting low androgen signaling, reminiscent of what is observed in the pathogenesis and therapeutic resistance of human BPH. Thus, although the involvement of PRL/STAT5 in human BPH remains to be established,[17] the Pb-PRL mouse is a useful preclinical BPH model to investigate the mechanisms contributing to disease development, including cell plasticity, and to challenge new therapeutic strategies as recently shown for anti-inflammatory compounds,[34] and in this study, for antioxidant therapy.

Acknowledgments

We thank the personnel of the technological core facilities including animal housing (Sarah Nadjah, Emilie Panafieu, Pierre Chérel, Olivier Claude), cytometry (Jérôme Mégret, Corinne Cordier), and histology (Sophie Berissi) of the SFR Necker (US24/UAR3633), and Sebastien Jacques from the Genom'IC facility of Cochin institute. We also thank Dr. Lucila Sackmann Sala for sharing bulk transcriptomic data of Pb-PRL mouse prostate epithelial cells, and Dr. Mitsuharu Yoshiyama for help with urodynamic studies and for critical reading of the manuscript.

Conflict of interest statement

O. Petitjean holds a patent on ATT repositioning for BPH treatment. He participated in initial study design, but had no role in data collection, analysis and interpretation, and report writing.

Author Contribution Statement

L.D.S., O.P., A.H., M.M., J.-E.G., and V.G. conceived the study. L.D.S., E.P., S.D., M.L., N.P., M.B., E.N., F.B., and I.N. performed cell and animal experiments. L.D.S., F.C., N.C., and M.M. performed bioinformatic analyses. L.D.S., F.C., F.B., M.M., S.P., J.-E.G., and V.G. validated the data. Original manuscript draft and figures were prepared by L.D.S., F.C., N.C., F.B., S.P., J.-E.G., and V.G. All authors (but O.P.) were involved in writing the paper and had final approval of the submitted and published versions. Project supervision and administration were carried out by L.D.S., M.M., J.-E.G., and V.G. Funds were acquired by V.G.

Supplemental Data

Supplemental material for this article can be found at *http://doi.org/10.1016/j.ajpath.2023.09.010*.

References

1. Lee CH, Akin-Olugbade O, Kirschenbaum A: Overview of prostate anatomy, histology, and pathology. Endocrinol Metab Clin North Am 2011, 40:565–575. viii-ix
2. Strand DW, Costa DN, Francis F, Ricke WA, Roehrborn CG: Targeting phenotypic heterogeneity in benign prostatic hyperplasia. Differentiation 2017, 96:49–61
3. Devlin CM, Simms MS, Maitland NJ: Benign prostatic hyperplasia - what do we know? BJU Int 2020, 127:389–399
4. Steers WD: 5alpha-reductase activity in the prostate. Urology 2001, 58 Suppl 1:17–24
5. McConnell JD, Roehrborn CG, Bautista OM, Andriole GL Jr, Dixon CM, Kusek JW, Lepor H, McVary KT, Nyberg LM Jr, Clarke HS, Crawford ED, Diokno A, Foley JP, Foster HE, Jacobs SC, Kaplan SA, Kreder KJ, Lieber MM, Lucia MS, Miller GJ, Menon M, Milam DF, Ramsdell JW, Schenkman NS, Slawin KM, Smith JA: The long-term effect of doxazosin, finasteride, and combination therapy on the clinical progression of benign prostatic hyperplasia. N Engl J Med 2003, 349:2387–2398
6. Roehrborn CG, Siami P, Barkin J, Damião R, Major-Walker K, Nandy I, Morrill BB, Gagnier RP, Montorsi F; CombAT Study Group: The effects of combination therapy with dutasteride and tamsulosin on clinical outcomes in men with symptomatic benign prostatic hyperplasia: 4-year results from the CombAT study. Eur Urol 2010, 57:123–131
7. Yu Z-J, Yan H-L, Xu F-H, Chao H-C, Deng L-H, Xu X-D, Huang J-B, Zeng T: Efficacy and side effects of drugs commonly used for the treatment of lower urinary tract symptoms associated with benign prostatic hyperplasia. Front Pharmacol 2020, 11:658
8. Rusu ME, Fizesan I, Vlase L, Popa DS: Antioxidants in age-related diseases and anti-aging strategies. Antioxidants (Basel) 2022, 11:1868
9. Minciullo PL, Inferrera A, Navarra M, Calapai G, Magno C, Gangemi S: Oxidative stress in benign prostatic hyperplasia: a systematic review. Urol Int 2015, 94:249–254
10. Zabaiou N, Mabed D, Lobaccaro JM, Lahouel M: Oxidative stress in benign prostate hyperplasia. Andrologia 2016, 48:69–73
11. Srivastava DSL, Mittal RD: Free radical injury and antioxidant status in patients with benign prostate hyperplasia and prostate cancer. Indian J Clin Biochem 2005, 20:162–165
12. Merendino RA, Salvo F, Saija A, Di Pasquale G, Tomaino A, Minciullo PL, Fraccica G, Gangemi S: Malondialdehyde in benign prostate hypertrophy: a useful marker? Mediators Inflamm 2003, 12:127–128
13. Olinski R, Zastawny TH, Foksinski M, Barecki A, Dizdaroglu M: DNA base modifications and antioxidant enzyme activities in human benign prostatic hyperplasia. Free Radic Biol Med 1995, 18:807–813
14. Vital P, Castro P, Ittmann M: Oxidative stress promotes benign prostatic hyperplasia. Prostate 2016, 76:58–67
15. Kindblom J, Dillner K, Sahlin L, Robertson F, Ormandy C, Tornell J, Wennbo H: Prostate hyperplasia in a transgenic mouse with prostate-specific expression of prolactin. Endocrinology 2003, 144:2269–2278
16. Nevalainen MT, Valve EM, Ingleton PM, Nurmi M, Martikainen PM, Harkonen PL: Prolactin and prolactin receptors are expressed and functioning in human prostate. J Clin Invest 1997, 99:618–627
17. Goffin V, Hoang DT, Bogorad RL, Nevalainen MT: Prolactin regulation of the prostate gland: a female player in a male game. Nat Rev Urol 2011, 8:597–607
18. Bernichtein S, Pigat N, Capiod T, Boutillon F, Verkarre V, Camparo P, Viltard M, Mejean A, Oudard S, Souberbielle JC, Friedlander G, Goffin V: High milk consumption does not affect prostate tumor progression in two mouse models of benign and neoplastic lesions. PLoS One 2015, 10:e0125423
19. Rouet V, Bogorad RL, Kayser C, Kessal K, Genestie C, Bardier A, Grattan DR, Kelder B, Kopchick JJ, Kelly PA, Goffin V: Local

prolactin is a target to prevent expansion of basal/stem cells in prostate tumors. Proc Natl Acad Sci U S A 2010, 107:15199−15204
20. Pigat N, Reyes-Gomez E, Boutillon F, Palea S, Barry Delongchamps N, Koch E, Goffin V: Combined sabal and urtica extracts (WS((R)) 1541) exert anti-proliferative and anti-inflammatory effects in a mouse model of benign prostate hyperplasia. Front Pharmacol 2019, 10:311
21. Bernichtein S, Pigat N, Camparo P, Latil A, Viltard M, Friedlander G, Goffin V: Anti-inflammatory properties of lipidosterolic extract of Serenoa repens (Permixon®) in a mouse model of prostate hyperplasia. Prostate 2015, 75:706−722
22. Boutillon F, Pigat N, Sala LS, Reyes-Gomez E, Moriggl R, Guidotti JE, Goffin V: STAT5a/b deficiency delays, but does not prevent, prolactin-driven prostate tumorigenesis in mice. Cancers (Basel) 2019, 11:929
23. Sackmann Sala L, Boutillon F, Menara G, De Goyon-Pelard A, Leprevost M, Codzamanian J, Lister N, Pencik J, Clark A, Cagnard N, Bole-Feysot C, Moriggl R, Risbridger GP, Taylor RA, Kenner L, Guidotti JE, Goffin V: A rare castration-resistant progenitor cell population is highly enriched in Pten-null prostate tumors. J Pathol 2017, 243:54−64
24. Sackmann-Sala L, Chiche A, Mosquera-Garrote N, Boutillon F, Cordier C, Pourmir I, Pascual-Mathey L, Kessal K, Pigat N, Camparo P, Goffin V: Prolactin-induced prostate tumorigenesis links sustained Stat5 signaling with the amplification of basal/stem cells and emergence of putative luminal progenitors. Am J Pathol 2014, 184:3105−3119
25. Kwon O-J, Choi JM, Zhang L, Jia D, Li Z, Zhang Y, Jung SY, Creighton CJ, Xin L: The Sca-1^{+} and Sca-1^{-} mouse prostatic luminal cell lineages are independently sustained. Stem Cells 2020, 38:1479−1491
26. Kwon OJ, Zhang L, Xin L: Stem cell antigen-1 identifies a distinct androgen-independent murine prostatic luminal cell lineage with bipotent potential. Stem Cells 2016, 34:191−202
27. Baures M, Puig Lombardi E, Di Martino D, Zeitouni W, Pacreau E, Dos Santos L, Dariane C, Boutillon F, Guidotti JE, Goffin V: Transcriptomic signature and growth factor regulation of castration-tolerant prostate luminal progenitor cells. Cancers (Basel) 2022, 14:3775
28. Baures M, Dariane C, Tika E, Puig Lombardi E, Barry Delongchamps N, Blanpain C, Guidotti JE, Goffin V: Prostate luminal progenitor cells: from mouse to human, from health to disease. Nat Rev Urol 2022, 19:201−218
29. Henry GH, Malewska A, Joseph DB, Malladi VS, Lee J, Torrealba J, Mauck RJ, Gahan JC, Raj GV, Roehrborn CG, Hon GC, MacConmara MP, Reese JC, Hutchinson RC, Vezina CM, Strand DW: A cellular anatomy of the normal adult human prostate and prostatic urethra. Cell Rep 2018, 25:3530−3542.e5
30. Joseph DB, Henry GH, Malewska A, Iqbal NS, Ruetten HM, Turco AE, Abler LL, Sandhu SK, Cadena MT, Malladi VS, Reese JC, Mauck RJ, Gahan JC, Hutchinson RC, Roehrborn CG, Baker LA, Vezina CM, Strand DW: Urethral luminal epithelia are castration-insensitive cells of the proximal prostate. Prostate 2020, 80:872−884
31. Yan Q, Wang M, Xia H, Dai C, Diao T, Wang Y, Hou H, Zhang H, Liu M, Long X: Single-cell RNA-sequencing technology demonstrates the heterogeneity between aged prostate peripheral and transitional zone. Clin Transl Med 2022, 12:e1084
32. Joseph DB, Henry GH, Malewska A, Reese JC, Mauck RJ, Gahan JC, Hutchinson RC, Mohler JL, Roehrborn CG, Strand DW: 5-alpha reductase inhibitors induce a prostate luminal to club cell transition in human benign prostatic hyperplasia. J Pathol 2022, 256:427−441
33. Zhang J, Zhang M, Tang J, Yin G, Long Z, He L, Zhou C, Luo L, Qi L, Wang L: Animal models of benign prostatic hyperplasia. Prostate Cancer Prostatic Dis 2021, 24:49−57
34. Vickman RE, Aaron-Brooks L, Zhang R, Lanman NA, Lapin B, Gil V, Greenberg M, Sasaki T, Cresswell GM, Broman MM, Paez JS, Petkewicz J, Talaty P, Helfand BT, Glaser AP, Wang CH, Franco OE, Ratliff TL, Nastiuk KL, Crawford SE, Hayward SW: TNF is a potential therapeutic target to suppress prostatic inflammation and hyperplasia in autoimmune disease. Nat Commun 2022, 13:2133
35. Lai K-P, Huang C-K, Fang L-Y, Izumi K, Lo C-W, Wood R, Kindblom J, Yeh S, Chang C: Targeting stromal androgen receptor suppresses prolactin-driven benign prostatic hyperplasia (BPH). Mol Endocrinol 2013, 27:1617−1631
36. He J, Qin T, Wen J, Qin F, Li F: An HPLC-MS/MS method for the quantitative determination of 4-hydroxy-anethole trithione in human plasma and its application to a pharmacokinetic study. J Pharm Biomed Anal 2011, 54:551−556
37. Yoshiyama M, Mochizuki T, Nakagomi H, Miyamoto T, Kira S, Mizumachi R, Sokabe T, Takayama Y, Tominaga M, Takeda M: Functional roles of TRPV1 and TRPV4 in control of lower urinary tract activity: dual analysis of behavior and reflex during the micturition cycle. Am J Physiol Renal Physiol 2015, 308:F1128−F1134
38. Sackmann-Sala L, Angelergues A, Boutillon F, d'Acremont B, Maidenberg M, Oudard S, Goffin V: Human and murine prostate basal/stem cells are not direct targets of prolactin. Gen Comp Endocrinol 2015, 220:133−142
39. Hao Y, Hao S, Andersen-Nissen E, Mauck WM 3rd, Zheng S, Butler A, Lee MJ, Wilk AJ, Darby C, Zager M, Hoffman P, Stoeckius M, Papalexi E, Mimitou EP, Jain J, Srivastava A, Stuart T, Fleming LM, Yeung B, Rogers AJ, McElrath JM, Blish CA, Gottardo R, Smibert P, Satija R: Integrated analysis of multimodal single-cell data. Cell 2021, 184:3573−3587.e29
40. Joseph DB, Henry GH, Malewska A, Reese JC, Mauck RJ, Gahan JC, Hutchinson RC, Malladi VS, Roehrborn CG, Vezina CM, Strand DW: Single-cell analysis of mouse and human prostate reveals novel fibroblasts with specialized distribution and microenvironment interactions. J Pathol 2021, 255:141−154
41. Korotkevich G, Sukhov V, Sergushichev A: Fast gene set enrichment analysis. bioRxiv 2019. doi:10.1101/060012, [Preprint]
42. Subramanian A, Tamayo P, Mootha VK, Mukherjee S, Ebert BL, Gillette MA, Paulovich A, Pomeroy SL, Golub TR, Lander ES, Mesirov JP: Gene set enrichment analysis: a knowledge-based approach for interpreting genome-wide expression profiles. Proc Natl Acad Sci U S A 2005, 102:15545−15550
43. Mootha VK, Lindgren CM, Eriksson KF, Subramanian A, Sihag S, Lehar J, Puigserver P, Carlsson E, Ridderstrale M, Laurila E, Houstis N, Daly MJ, Patterson N, Mesirov JP, Golub TR, Tamayo P, Spiegelman B, Lander ES, Hirschhorn JN, Altshuler D, Groop LC: PGC-1alpha-responsive genes involved in oxidative phosphorylation are coordinately downregulated in human diabetes. Nat Genet 2003, 34:267−273
44. Schaefer CF, Anthony K, Krupa S, Buchoff J, Day M, Hannay T, Buetow KH: PID: the pathway interaction database. Nucleic Acids Res 2009, 37:D674−D679
45. Andreatta M, Carmona SJ: UCell: robust and scalable single-cell gene signature scoring. Comput Struct Biotechnol J 2021, 19:3796−3798
46. La Manno G, Soldatov R, Zeisel A, Braun E, Hochgerner H, Petukhov V, Lidschreiber K, Kastriti ME, Lonnerberg P, Furlan A, Fan J, Borm LE, Liu Z, van Bruggen D, Guo J, He X, Barker R, Sundstrom E, Castelo-Branco G, Cramer P, Adameyko I, Linnarsson S, Kharchenko PV: RNA velocity of single cells. Nature 2018, 560:494−498
47. Bergen V, Lange M, Peidli S, Wolf FA, Theis FJ: Generalizing RNA velocity to transient cell states through dynamical modeling. Nat Biotechnol 2020, 38:1408−1414
48. Lukacs RU, Goldstein AS, Lawson DA, Cheng D, Witte ON: Isolation, cultivation and characterization of adult murine prostate stem cells. Nat Protoc 2010, 5:702−713
49. Drost J, Karthaus WR, Gao D, Driehuis E, Sawyers CL, Chen Y, Clevers H: Organoid culture systems for prostate epithelial and cancer tissue. Nat Protoc 2016, 11:347−358
50. Karthaus WR, Hofree M, Choi D, Linton EL, Turkekul M, Bejnood A, Carver B, Gopalan A, Abida W, Laudone V, Biton M,

FLA 5.6.0 DTD ■ AJPA3976_proof ■ 22 October 2023 ■ 9:32 am ■ EO: AJPA-D-23-

Chaudhary O, Xu T, Masilionis I, Manova K, Mazutis L, Pe'er D, Regev A, Sawyers CL: Regenerative potential of prostate luminal cells revealed by single-cell analysis. Science 2020, 368:497−505

51. Crowley L, Cambuli F, Aparicio L, Shibata M, Robinson BD, Xuan S, Li W, Hibshoosh H, Loda M, Rabadan R, Shen MM: A single-cell atlas of the mouse and human prostate reveals heterogeneity and conservation of epithelial progenitors. Elife 2020, 9:e59465
52. Kwon OJ, Zhang Y, Li Y, Wei X, Zhang L, Chen R, Creighton CJ, Xin L: Functional heterogeneity of mouse prostate stromal cells revealed by single-cell RNA-Seq. iScience 2019, 13:328−338
53. Mulholland DJ, Tran LM, Li Y, Cai H, Morim A, Wang S, Plaisier S, Garraway IP, Huang J, Graeber TG, Wu H: Cell autonomous role of PTEN in regulating castration-resistant prostate cancer growth. Cancer Cell 2011, 19:792−804
54. Chan JM, Zaidi S, Love JR, Zhao JL, Setty M, Wadosky KM, Gopalan A, Choo ZN, Persad S, Choi J, LaClair J, Lawrence KE, Chaudhary O, Xu T, Masilionis I, Linkov I, Wang S, Lee C, Barlas A, Morris MJ, Mazutis L, Chaligne R, Chen Y, Goodrich DW, Karthaus WR, Pe'er D, Sawyers CL: Lineage plasticity in prostate cancer depends on JAK/STAT inflammatory signaling. Science 2022, 377:1180−1191
55. Pouzaud F, Christen MO, Warnet JM, Rat P: [Anethole dithiolethione: an antioxidant agent against tenotoxicity induced by fluoroquinolones]. Pathol Biol (Paris) 2004, 52:308−313
56. Detaille D, Pasdois P, Semont A, Dos Santos P, Diolez P: An old medicine as a new drug to prevent mitochondrial complex I from producing oxygen radicals. PLoS One 2019, 14:e0216385
57. Hayward SW, Dahiya R, Cunha GR, Bartek J, Deshpande N, Narayan P: Establishment and characterization of an immortalized but non-transformed human prostate epithelial cell line: BPH-1. In Vitro Cell Dev Biol Anim 1995, 31:14−24
58. Crowell PD, Fox JJ, Hashimoto T, Diaz JA, Navarro HI, Henry GH, Feldmar BA, Lowe MG, Garcia AJ, Wu YE, Sajed DP, Strand DW, Goldstein AS: Expansion of luminal progenitor cells in the aging mouse and human prostate. Cell Rep 2019, 28:1499−1510.e6
59. Liu X, Grogan TR, Hieronymus H, Hashimoto T, Mottahedeh J, Cheng D, Zhang L, Huang K, Stoyanova T, Park JW, Shkhyan RO, Nowroozizadeh B, Rettig MB, Sawyers CL, Elashoff D, Horvath S, Huang J, Witte ON, Goldstein AS: Low CD38 identifies progenitor-like inflammation-associated luminal cells that can initiate human prostate cancer and predict poor outcome. Cell Rep 2016, 17:2596−2606
60. Strand DW, Jiang M, Murphy TA, Yi Y, Konvinse KC, Franco OE, Wang Y, Young JD, Hayward SW: PPARgamma isoforms differentially regulate metabolic networks to mediate mouse prostatic epithelial differentiation. Cell Death Dis 2012, 3:e361
61. Federer-Gsponer JR, Muller DC, Zellweger T, Eggimann M, Marston K, Ruiz C, Seifert HH, Rentsch CA, Bubendorf L, Le Magnen C: Patterns of stemness-associated markers in the development of castration-resistant prostate cancer. Prostate 2020, 80:1108−1117
62. Burger PE, Gupta R, Xiong X, Ontiveros CS, Salm SN, Moscatelli D, Wilson EL: High aldehyde dehydrogenase activity: a novel functional marker of murine prostate stem/progenitor cells. Stem Cells 2009, 27:2220−2228
63. Freeland J, Crowell PD, Giafaglione JM, Boutros PC, Goldstein AS: Aging of the progenitor cells that initiate prostate cancer. Cancer Lett 2021, 515:28−35
64. Harman SM, Metter EJ, Tobin JD, Pearson J, Blackman MR; Baltimore Longitudinal Study of Aging: Longitudinal effects of aging on serum total and free testosterone levels in healthy men. Baltimore Longitudinal Study of Aging. J Clin Endocrinol Metab 2001, 86:724−731
65. Yang Y, Hu S, Liu J, Cui Y, Fan Y, Lv T, Liu L, Li J, He Q, Han W, Yu W, Sun Y, Jin J: CD8+ T cells promote proliferation of benign prostatic hyperplasia epithelial cells under low androgen level via modulation of CCL5/STAT5/CCND1 signaling pathway. Sci Rep 2017, 7:42893
66. Jin B-R, Lim C-Y, Kim H-J, Lee M, An H-J: Antioxidant mitoquinone suppresses benign prostatic hyperplasia by regulating the AR-NLRP3 pathway. Redox Biol 2023, 65:102816
67. Jin B-R, Kim H-J, Na J-H, Lee W-K, An H-J: Targeting benign prostate hyperplasia treatments: AR/TGF-beta/NOX4 inhibition by apocynin suppresses inflammation and proliferation. J Adv Res 2023. doi:10.1016/j.jare.2023.04.006, [Epub ahead of print] Q30
68. Nagano T, Takeyama M: Enhancement of salivary secretion and neuropeptide (substance P, alpha-calcitonin gene-related peptide) levels in saliva by chronic anethole trithione treatment. J Pharm Pharmacol 2001, 53:1697−1702
69. Schiødt M, Oxholm P, Jacobsen A: Treatment of xerostomia in patients with primary Sjogren's syndrome with sulfarlem. Scand J Rheumatol Suppl 1986, 61:250−252
70. Parisotto M, Metzger D: Genetically engineered mouse models of prostate cancer. Mol Oncol 2013, 7:190−205
71. Roberts RO, Jacobson DJ, Rhodes T, Klee GG, Leiber MM, Jacobsen SJ: Serum sex hormones and measures of benign prostatic hyperplasia. Prostate 2004, 61:124−131